Solar Absorption in Clouds of Finite Horizontal Extent

J.M. Davis, S.K. Cox, and T.B. McKee

Department of Atmospheric Science
Colorado State University
Fort Collins, Colorado

Colorado State University

Department of Atmospheric Science

Paper No. 282

SOLAR ABSORPTION IN CLOUDS OF FINITE HORIZONTAL EXTENT

by

John M. Davis, Stephen K. Cox and Thomas B. McKee

Research Report supported by
The Global Atmospheric Research Program,
National Science Foundation and the
GATE Project office, NOAA under grants
OCD -74-21678 and ATM 77-15369

Department of Atmospheric Science
Colorado State University
Fort Collins, Colorado
80523

January, 1978

Atmospheric Science Paper No. 282

ABSTRACT

SOLAR ABSORPTION IN CLOUDS OF FINITE HORIZONTAL EXTENT

A model for incorporating droplet and water vapor absorption into finite cloud, radiative transfer calculations is described. Theoretical values of directional reflectance, absorption of solar radiation above, in and below cloud level, and downward scattered radiant power are calculated for infinite and finite cloud volume elements and the results are compared. Absorption in the regions on the solar and anti-solar sides of the finite cloud is also calculated.

Directional reflectance values for finite clouds are less than for the corresponding infinite cloud volume elements. Absorption within the finite cloud elements may be smaller or greater than in infinite cloud elements depending upon zenith angle. Radiant power scattered into the downward hemisphere is greater for the finite cloud case than for the infinite cloud.

The effects of finite cloud radiative transfer upon estimates of areal directional reflectance, surface solar irradiance, total absorption in the atmosphere, and a cloud topped mixed layer model are assessed. Areal directional reflectance estimates for cloud fields over a totally absorbing surface and estimates of surface solar irradiance using finite cloud results are greater than or less than corresponding values calculated using infinite cloud results, depending on zenith angle.

The time averaged disposition of solar radiation is calculated as a function of latitude for a 20% cloud cover over a totally absorbing surface for solar geometries corresponding to the equinox and the summer and winter solstices. The results indicate greater amounts of reflected and smaller amounts of transmitted radiant power for the cloud field in

nearly all cases when finite cloud properties are assumed than when infinite cloud characteristics are used. Amounts of radiant power absorbed in the two cases are nearly equal.

The importance of distinguishing between horizontal and vertical cloud dimensions in estimating finite cloud cover amounts from satellite imagery is discussed. A calculation of the time averaged reflectivity, absorptivity and transmissivity of a region characterized by a totally absorbing surface underlying a finite cloud field indicates reflectivity is overestimated and transmissivity is underestimated, especially in middle latitudes, if vertical and horizontal cloud dimensions are not distinguished in the satellite image. The calculation indicates that absorptivity is not greatly affected.

ACKNOWLEDGEMENTS

We would like to extend our sincere appreciation to Dr. Ronald M. Welch for his helpful suggestions. We would also like to thank Ms. M. C. Polifka for her aid in programming the model, and Ms. S. Wunch and Ms. P. Martin for typing this document.

TABLE OF CONTENTS

TABLE OF CONTENTS (Continued)

LIST OF TABLES

LIST OF TABLES (Continued)

LIST OF FIGURES

LIST OF FIGURES (Continued)

LIST OF FIGURES (Continued)

I.0 INTRODUCTION

An understanding of the interaction of solar radiation with the earth's atmosphere is essential to the solution of many problems in the atmospheric sciences. Determination of the planetary albedo of the earth, calculation of solar heating in the atmosphere and at the earth's surface, and inference of cloud parameters from satellite measurements are but a few examples. Theoretical investigations into the nature of this interaction address themselves to the solution of some form of the radiative transfer equation.

Until recently, such investigations have been limited to the solution of the radiative transfer equation in horizontally homogeneous semi-infinite atmospheres. Recent efforts, employing Monte Carlo techniques, have examined properties of finite clouds and clouds with horizontal inhomogeneities. Examples of such studies are found in Busygin et al. (1973), McKee and Cox (1974), McKee and Cox (1976), Van Blerkom (1971) and Wendling (1977). These studies examine such parameters as cloud directional reflectance and radiance patterns for different cloud shapes as a function of cloud optical thickness and cloud-sun geometry. Results of these studies indicate that the directional reflectance of finite clouds is generally lower than that of semi-infinite clouds of the same optical thickness. Radiance values for the finite cloud can be higher or lower than for the corresponding infinite case depending on the particular cloud-sun geometry.

Another aspect of the transfer problem which has received recent attention is the absorption of solar radiation by vapors, aerosols and water droplets. In particular, few computational results have been

presented showing the absorption profile for solar radiation within clouds. Liou and Sasamori (1975), present a detailed calculation of solar absorption in clear and hazy atmospheres as a function of solar geometry and surface albedo. Calculated absorption for a hazy atmosphere is shown to be as high as 30%. Twomey (1976), examines solar absorption in continental and maritime water cloud models and also for an ice cloud model and concludes, that for moderately thick clouds (1 km), absorption is about 15% at high solar elevations. Welch et al. (1976), present a detailed account of radiation parameters calculated for clouds of varying thickness and height in the atmosphere, subject to changes in the surface albedo, solar zenith angle and liquid water content. Of particular note are in-cloud absorption profiles which result in solar heating great enough to be considered significant in dynamic weather prediction models. All of these latter studies employ horizontally infinite cloud models.

The goal of the present study is to investigate solar absorption in clouds of finite horizontal extent. The model used calculates various parameters such as cloud directional reflectance and solar absorption. Radiance fields are not calculated. One objective of the study is to determine if including absorption in the calculation of cloud directional reflectance alters the prediction that finite clouds have lower values of this parameter than do infinite clouds of the same optical thickness. Also, a comparison is made between absorption values in finite clouds and those in infinite clouds of the same optical thickness. This latter comparison is not limited to the cloud region itself but is also carried out for the atmosphere above and below the cloud. In addition, a comparison is made between values of absorption

in the atmosphere surrounding the finite cloud and an equivalent cloud free layer in order to obtain the magnitude of solar heating outside the cloud caused by its presence in the atmospheric layer.

2.0 DESCRIPTION OF THE MODEL

Basically, the model consists of a band and droplet absorption calculation superimposed on a Monte Carlo scattering routine. The scattering routine is employed to record the paths of photons undergoing pure scattering by cloud water droplets. Next, the absorption scheme simulates absorption of photons from the top of the atmosphere to the point of entry into the cloud and uses the pre-recorded photon paths to obtain in-cloud vapor and droplet absorptions. Finally, photon trajectories are simulated from point of cloud exit to exit from the atmosphere, either at the upper limit or at the earth's surface, in order to complete the absorption profile.

2.1 Monte Carlo scattering model

The scattering model closely resembles that presented by McKee and Cox (1974). A rectangular parallelepiped cloud region is specified with the coordinate origin located at the center of the top face. The region is subdivided by defining mutually perpendicular intersecting planes inside the larger parallelepiped, thus defining boxes within the larger cloud region, (see Figure 5). By assigning appropriate cloud parameters to selected boxes, a cloud of the desired shape is constructed. Photon entry points are distributed in a uniform manner on the top face of the larger cloud region. A photon enters the cloud region with a specified solar zenith and azimuth angle and continues until it has traversed a distance s at which point a scattering event occurs. The distance s is given as the solution to the equation

$$T = e^{-\tau} = \exp(-\Sigma\, \beta_i \cdot s_i) \qquad (1)$$

where T is the transmissivity of the path s, τ the optical depth, and β_i is the volume extinction coefficient of the ith cloud box. Since T is the probability that a photon travels a distance s between scattering events, a random number can be chosen for T, and s can be determined by summing along the photon path until the right hand side equals the given random number. At this point a scattering is simulated and a new direction of travel is determined by selecting values for the Eulerian angles α and γ relative to the old direction. If the photon was travelling along the z' axis in an x'y'z' coordinate system, the angle γ represents a counter clockwise rotation of the x'y' coordinate axes about the z' axis to generate new x"y" axes. The value for γ is selected from a uniform angular distribution ranging from 0 to 2π. The new direction of propagation is along the z" axis which is obtained by a counter clockwise rotation of the z' and y" axes about the x" axis through the angle α. The probability of a photon being scattered between 0 and the angle α is given by the normalized integral over solid angle of the scattering phase function $P(\alpha)$. In the Monte Carlo routine a random number between 0 and 1 is assigned to this probability and α is then given as the solution to

$$PP(\alpha) = \frac{\int_0^{\alpha} P(\alpha) \sin \alpha \, d\alpha}{\int_0^{\pi} P(\alpha) \sin \alpha \, d\alpha} \qquad (2)$$

where $PP(\alpha)$ has the value of the random number.

2.2 Absorption technique

The absorption by water vapor is calculated according to the empirical fit of Howard, Burch and Williams (1956), in a form modified by Liou and Sasamori (1975). The mean fractional absorptivity A in the band of width $\Delta\nu$ (cm^{-1}) is given by

$$A = \frac{1}{\Delta\nu} [C + D \log_{10} (x + x_0)], \tag{3}$$

where $$x = \mu p_{eff}^{K/D},$$

and $$x_0 = 10^{-C/D}.$$

In the above formula K, C and D are empirically derived constants, μ is the optical path of water vapor in precipitable centimeters and p_{eff} is the effective pressure of the path in mm Hg.

Each photon is assigned the average extra-terrestrial radiant power characteristic of the band in question. The change in mean fractional absorptivity is calculated for a segment of the photon trajectory and the product of this change with the radiant power assigned to the photon is calculated. The sum of all such products for the path segments in a certain region divided by the total number of photons incident on the region results in the radiant power absorbed in the region.

Absorption due to water droplets is accounted for by using a simple weighting scheme. If a photon has an energy E_0 before a scattering event, then the fraction of the surviving energy after scattering is given by the product ωE_0 where ω is the single particle scattering albedo.

As the photon path is traced through the cloud boxes, the photon's energy is successively decreased by fractional absorptions due to water vapor and droplets respectively. In this way, the photon enters each interaction with the proper amount of energy.

The hybrid model described above appears at first to be a significant departure from the pure Monte Carlo approach. However, as envisioned here, the technique is merely an extension of the original method. In the original Monte Carlo calculation each photon traces out a certain path through the cloud due to pure scattering. If the number of photons was extremely large, it would be likely that groups of photons could be found that followed similar, although not necessarily identical, paths through the cloud boxes. If absorption by vapor and cloud droplets is now included some of the photons in each of these groups will be selectively absorbed by the gas and the droplets. The profile for these processes is exactly that given by the band model for the gaseous case and the weighting scheme for the droplet case.

When discussing the absorption of solar radiation in finite cloud structures it is necessary to clarify exactly what is meant when using the units of power per unit area. In an infinite cloud calculation these units are convenient because they allow for simple conversion to heating rates in units of degrees per unit time. There is no ambiguity in infinite cloud calculations since the area on which the radiation is incident is also the horizontal bounding area of the volume being heated by the solar energy. This is not necessarily the case when one considers finite structures. A finite cloud, for example, can absorb solar energy which was not incident on the top of the cloud. In this case the units of power per unit area are somewhat ambiguous because there may be

two different areas involved; one on which the radiation was incident and one which bounds the volume in which the energy is being absorbed. For this reason, in this research, the units of power per unit area shall always refer to the radiant power absorbed in a volume element divided by the horizontal surface area bounding this element. Thereby, the usual conversions to heating rates may be employed.

2.3 Partitioning of the near infra-red spectrum

Once the cloud geometry, the volume extinction coefficient and the phase function are specified, the photon trajectories are essentially established for a given random number sequence. The extinction coefficient and the phase function are frequency dependent, however, so that ideally many Monte Carlo computations should be made for a particular wavelength interval. Computer time considerations prohibit this. Instead, an approximation identical to that given in Welch et al. (1976), is used to divide the near infra-red wavelength spectrum into two different regions. The first of these is characterized by strong vapor absorption while in the second the droplet absorption is predominant. A single volume extinction coefficient and phase function are assigned to each of these regions by weighting several volume extinction coefficients and several sets of phase function expansion coefficients according to the magnitude of the extraterrestrial solar intensity at various wavelengths within the respective regions. The original extraterrestrial solar intensities, volume extinction coefficients and Legendre expansion coefficients are given in Zdunkowski et al. (1967). Table 1 shows the properties of the two regions, and Figs. 1 to 4 show the derived phase functions [P (α)] and the

corresponding normalized integrated phase function [PP (α)]. The Legendre expansion coefficients are representative of a Best droplet distribution for a liquid water content of 0.1 g/m^3. Also shown in Table I are the single particle scattering albedos which were calculated in a manner similar to that of the volume extinction coefficients. However, the model does provide for the use of several scattering albedos in the determination of droplet absorption, so that these were computed for band intervals rather than the larger region interval.

In the manner just described it is possible to approximate scattering due to cloud droplets and absorption due to water vapor and cloud droplets for the near infra-red solar spectrum by using two Monte Carlo calculations and two photon tracking routines.

It is noted here that Rayleigh scattering is not included in the model. This effect has been omitted because at the wavelengths in question the coefficient for Rayleigh scattering is several orders of magnitude smaller than those for Mie scattering employed in the model.

Also, the calculations have been limited to the near infra-red portion of the solar spectrum since it is in this portion of the spectrum that most of the absorption of solar radiation takes place.

2.4 Finite mode and infinite mode

As discussed up to this point the model simulates radiative transfer in finite clouds. In order to make many of the comparisons in this study, it is necessary to calculate certain radiative parameters for finite clouds and for infinite clouds of the same optical thickness. The infinite cloud calculation is essentially the same as that for the finite cloud up to the point of photon exit from the cloud. At this

Region	Wavelength Interval in Micrometers	Wavelength (μm) of H_2O Vapor Band Centers Included in Region	Derived Single Particle Scattering Albedos Over Band Regions	Volume Extinction Coefficients (km^{-1})
I	.80 - 2.7	.94 1.10 1.38 1.87	.99990825 .99976674 .99566914 .98886346	36.01
II	2.7 - 8.0	2.70 3.30 6.30	.83709146 .57787098 .59735099	39.36

Table 1. Wavelength intervals, water vapor band center wavelengths, single particle scattering albedos and volume extinction coefficients for the two near infra-red band regions.

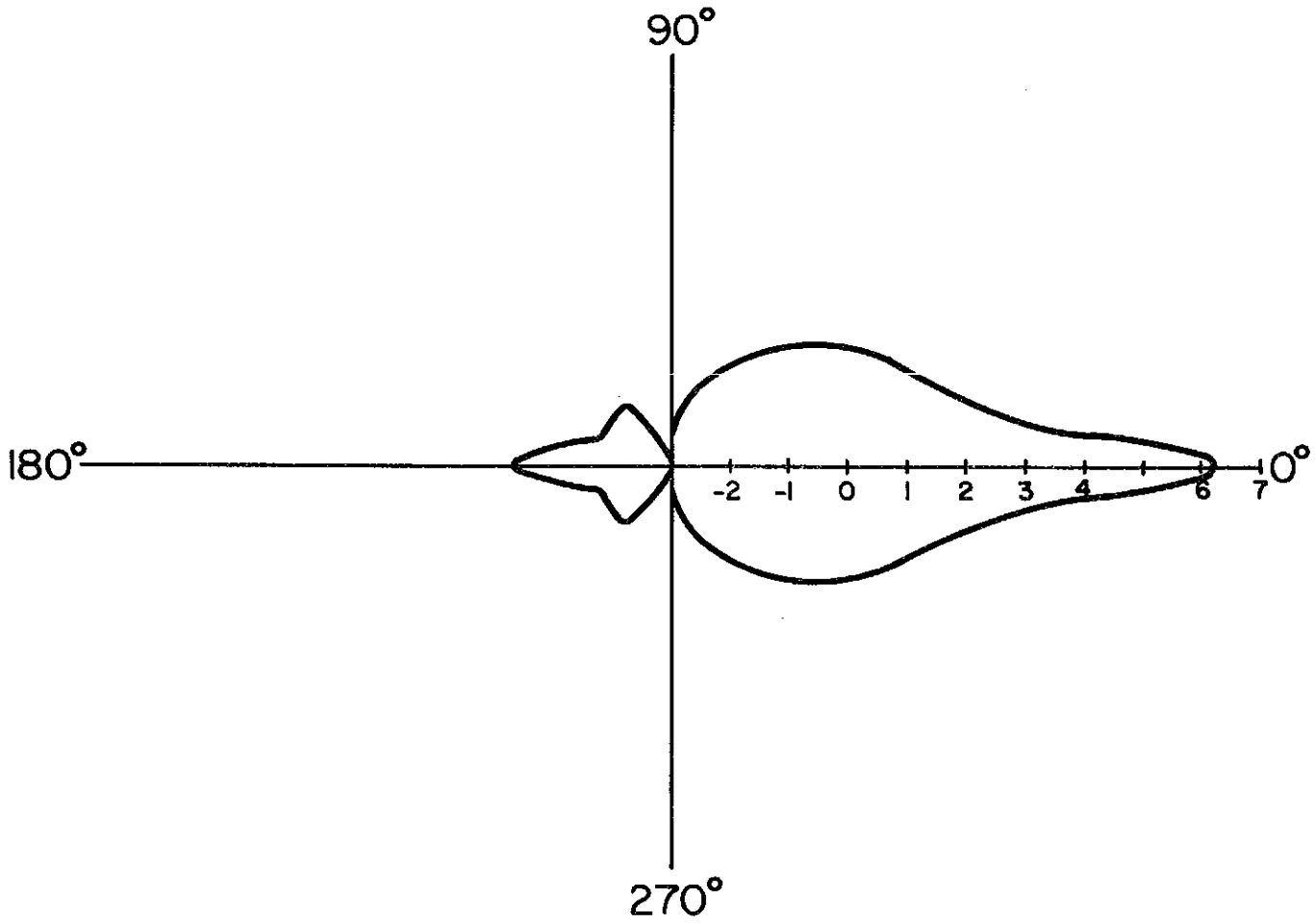

Figure 1. Natural logarithm of the phase function $P(\alpha)$ for region I as a function of propagation angle α.

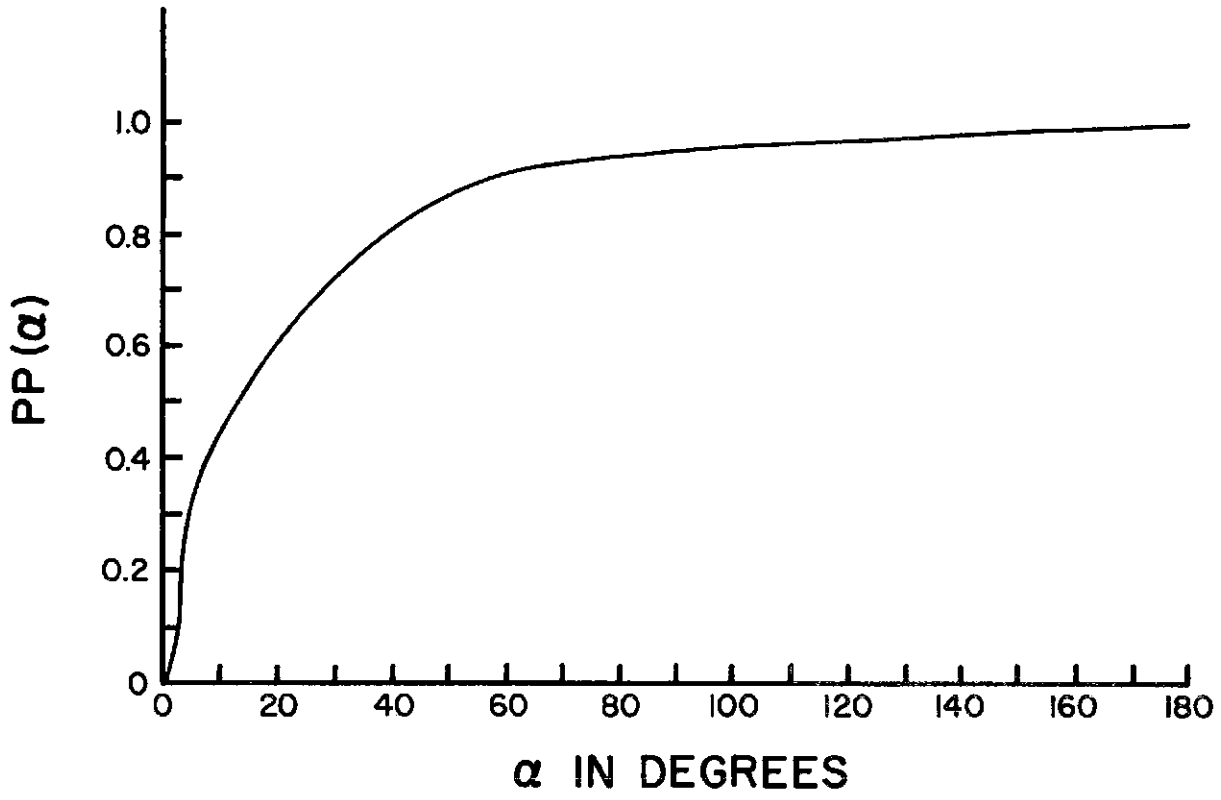

Figure 2. Normalized integrated phase function PP(α) for region I as a function of the propagation angle α.

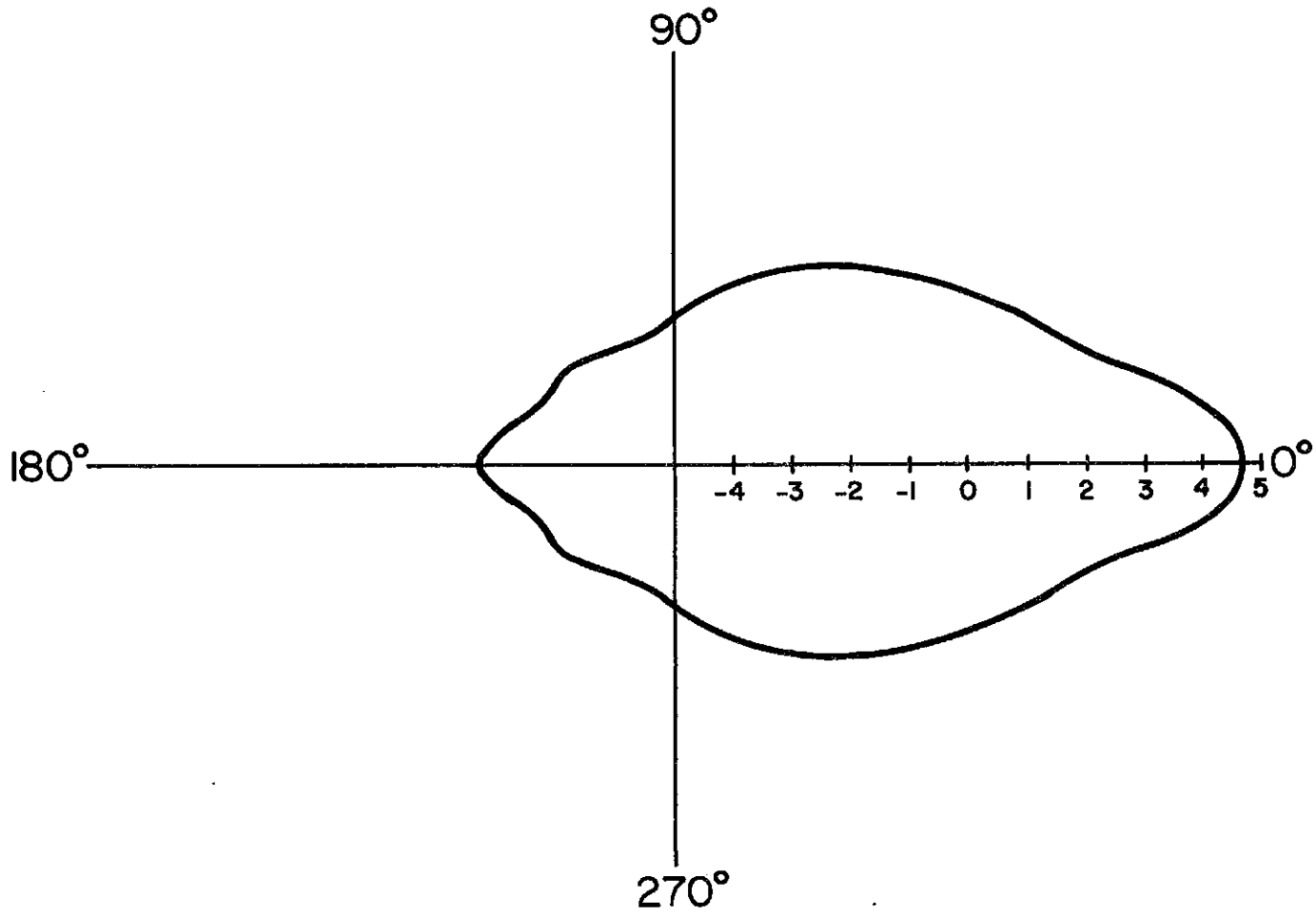

Figure 3. Natural logarithm of the phase function $P(\alpha)$ for region II as a function of propagation angle α.

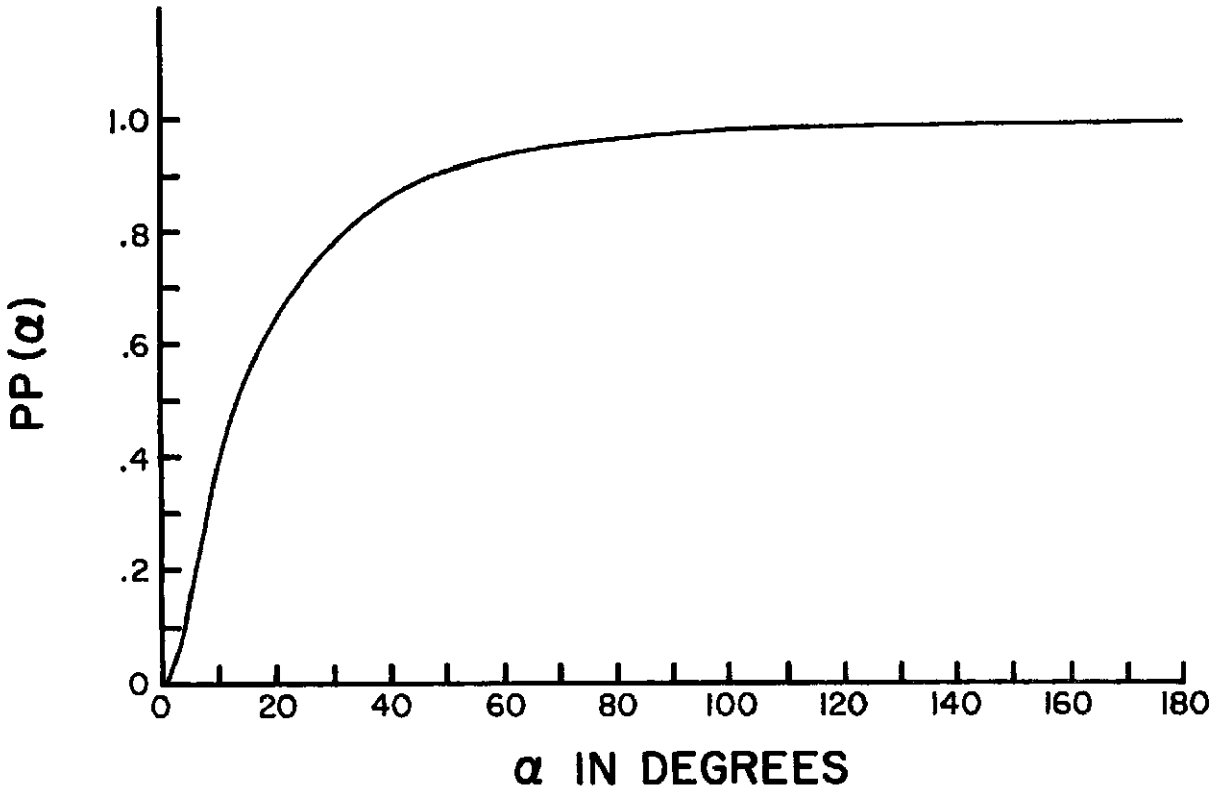

Figure 4. Normalized integrated phase function PP(α) for region II as a function of propagation angle α.

point, if the photon is exiting one of the vertical sides of an exterior cloud box, it is forced to re-enter the corresponding vertical face on the other side of the cloud without change of direction. For example, if the exit is through the $x = x_e$ plane, at the point (x_e, y, z), then the re-entry point is $(-x_e, y, z)$, and similarly for exits through the $y = y_e$ planes. In this way, photons escape only through the top and bottom faces, and a horizontally infinite cloud is simulated.

2.5 Advantages and disadvantages of the hybrid model

It should be acknowledged, at this point, that the hybrid model is not intended to be an operational tool. There are certain characteristics of the model which would make impractical incorporation of the model into one which is broader in scope. Firstly consider the amount of execution time. Monte Carlo routines require large amounts of machine time; the amount depending, in this case, on the number of photons processed and the optical thickness of the cloud. There is also a large amount of peripheral time required, which is associated with processing the magnetic tapes on which the photon paths are recorded. Secondly, there is a limitation to how many photon paths can be recorded on a given length of magnetic tape. As the cloud's optical thickness increases, so does the number of photon path segments, from scattering to scattering, until the photon exits the cloud. For clouds of 1 km thickness, for example, a sizable fraction of the photons will undergo several hundred scatterings each before exiting the cloud. Consequently the hybrid model is practically limited to studies of the absorptive properties of finite and infinite clouds which are optically thin.

There are certain advantages, however, of the hybrid model when used within its limitations. Once the photon paths are established,

various properties of the cloud-atmosphere system may be changed and new results obtained, without expending additional machine time for another Monte Carlo computation. For example, if the scattering is assumed to be nearly independent of cloud temperature, the absorption can be examined with the cloud in any of several different atmospheres. Water vapor in the cloud can also be adjusted as well as the cloud's height in the atmosphere. Additionally, desired statistical parameters concerning photon path lengths, scattering angles or points of cloud exit are easily obtained. Finally, the relative contributions of vapor and droplet absorptions may be examined as a function of variation of any of the above mentioned variables.

3.0 SPECIFICATION OF AN ATMOSPHERE AND CLOUD TYPES

In the subsequent sections two basic cloud structures and one atmosphere are used. Calculations are performed for cubic clouds 210 m (τ = 7.15) and 630 m (τ = 21.45) thick as well as for the corresponding 210 m and 630 m thick infinite clouds. When the clouds are immersed in an atmosphere, the U.S. Standard Tropical Atmosphere of 1962 as presented in McClatchey et al. (1971) is used. Cloud top for both clouds is 1.5 km and a saturation water vapor density of 15.7 g/m^3 is specified. A surface albedo of 0 is assumed in all cases. Calculations are made for solar zenith angles of 0°, 30° and 60°. Both the horizontally infinite and the finite clouds are divided into three equal layers. In addition, the finite clouds and corresponding infinite cloud volumes are resolved into sub-cloud cubical boxes of the same dimension as the thickness of the cloud layers. This results in the finite cloud and the corresponding infinite cloud volume being sub-divided into 27 cubes. When the finite cloud is immersed in the atmosphere, it is bordered on each of two sides by additional boxes of clear atmosphere, in order to allow for the examination of absorption of solar radiation near the cloud on the solar and anti-solar sides, and also, to allow for the proper optical path summation for photons entering the cloud at the 30° and 60° zenith angles, see Figure 5.

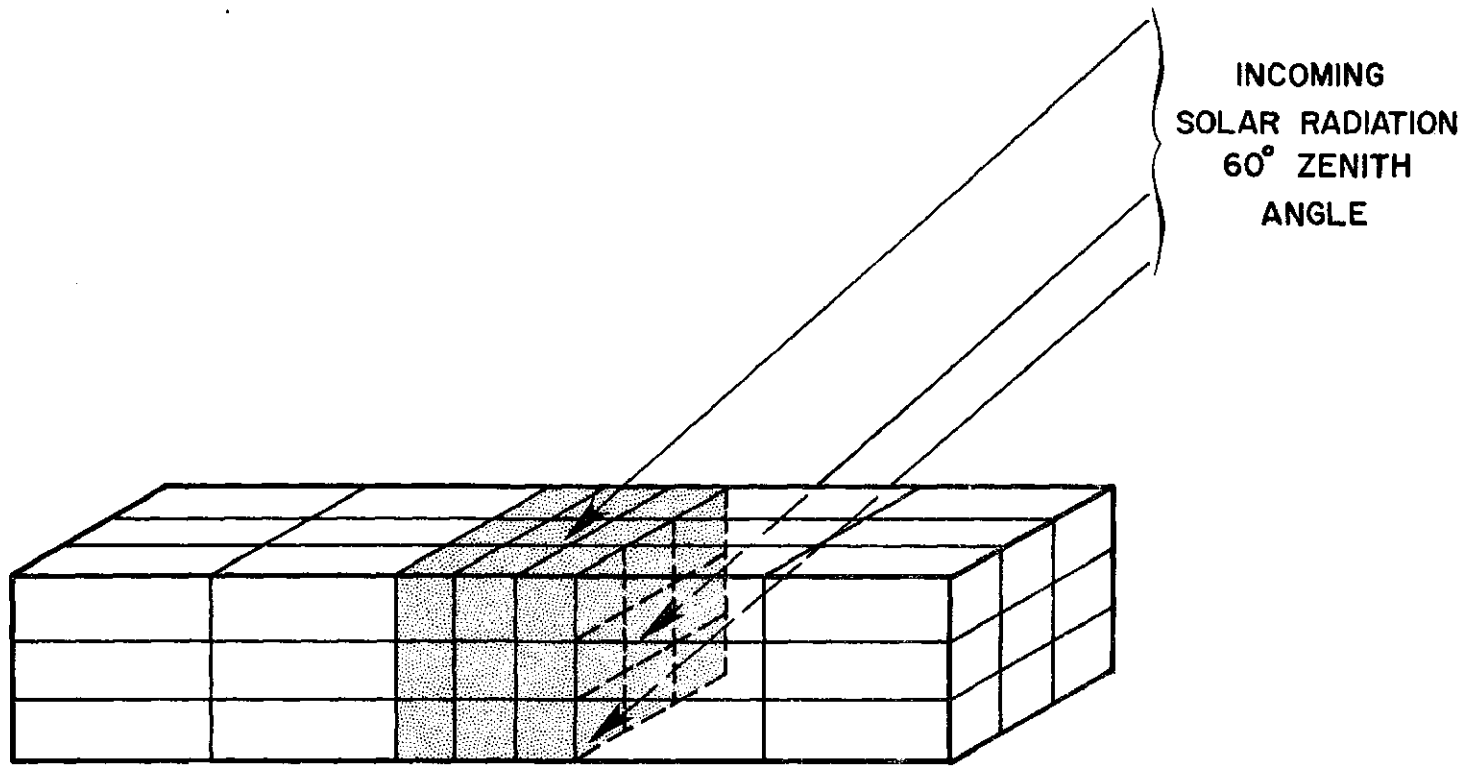

Figure 5. Structure of the finite cloud (stipled volume) and surrounding clear region in relation to the incoming solar radiation.

4.0 PRECISION AND ACCURACY OF THE RESULTS

The precision to which any quantity may be calculated by a Monte Carlo method is proportional to the square root of the number of photons used in the simulation. In the present calculations the values of absorbed solar radiation in the finite cloud boxes have been derived from a smaller number of photon trajectories than any other calculated parameter. Examination of the convergence of these numbers toward some mean value gives a worst case indication of the amount of noise in the calculation. Such an examination is most conveniently provided by taking advantage of symmetries which exist in the 0° zenith angle calculation. For example, it is clear that in this case each of the corner boxes in a particular layer should absorb the same amount of radiant power. This is also true of the four boxes in each layer between the corner boxes. An experiment was carried out at the outset of this research in order to determine the number of photons necessary to achieve reasonable precision. In the experiment the model was applied to a 24 km by 24 km by 210 m thick cloud and the standard deviation of the symmetrical absorption values calculated. Figure 6 shows a plot of these standard deviations expressed as a percent of the mean of the symmetric absorption values. On the basis of this test the figure of 20,000 photons was adopted for purposes of this research.

A continual check was made of similar errors in the infinite cloud calculations which were subsequently performed. The most serious errors were found for the bottom layer of the cloud where little energy is available for absorption. For this layer, the r.m.s. error was typically 2.0% of the mean net flux divergence in that layer. Corresponding

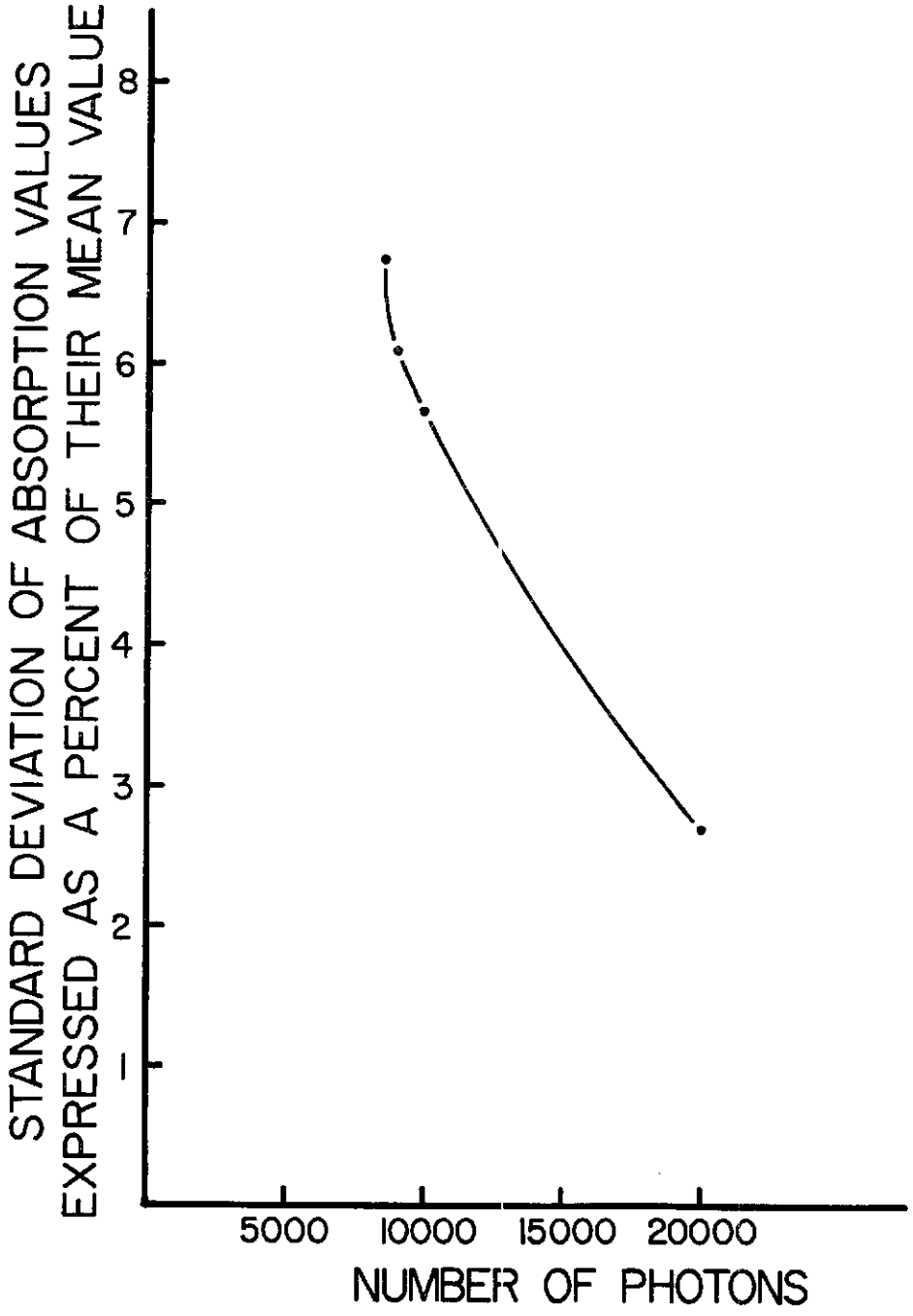

Figure 6. Standard deviation of absorption values expressed as a percent of their mean value vs. number of photons used in the calculation.

errors in the middle and top layers were 1.5% and .75% respectively.

No such check could be made for the finite cloud boxes, for the off-zenith cases, since only pairs of boxes exist in each layer which should exhibit the same absorption characteristics. In order to examine the precision for the off-zenith finite cloud case, the following check was made. Using the 630 m thick cloud geometry with a 60° solar zenith angle, including in-cloud as well as atmospheric absorption, three identical calculations were carried out with the exception of a change in the random number sequence. The precision of the results is then indicated by the consistency of the three calculations in predicting the various parameters. The largest discrepancy among the three pairs of results for all parameters of interest was noted. The largest percentage error, about 12%, was found in the net flux divergence values for the corner cloud boxes which receive the smallest irradiance, that is, the two outside boxes in the bottom cloud layer on the anti-solar side. The percentage error values were found to rapidly decrease in all the other cases. The remaining bottom layer boxes show errors on the order of 5% for the middle row and 2.5% for the bottom boxes on the solar side. For the top boxes, the values are typically near the 1% level. The largest discrepancy in the directional reflectance values resulted in 0.43% error with respect to the mean of the three values.

Verification of the accuracy of the model was accomplished by making a comparison between absorption values calculated by the hybrid model in the infinite mode, with corresponding values calculated by a doubling model. Both models were used to calculate the absorption profile within a 210 m thick (τ = 7.15) cloud, with zero surface albedo, no absorption above the cloud, a saturation water vapor density of

20 g/m^3, for a zenith angle of 0°, and using identical values for volume scattering coefficients, single particle scattering albedos and Legendre expansion coefficients. The results are shown in Table 2.

Cloud layer in meters	Solar absorption (hybrid method) in watts·m^{-2}	Solar absorption (doubling method) in watts·m^{-2}
210 - 140	155.0	155.0
140 - 70	50.9	51.6
70 - 0	25.1	24.8

Table 2. Comparison of absorption values calculated by the hybrid model with corresponding values from a doubling method calculation.

Generally, this study consists of comparisons between parameters calculated for finite clouds and identical parameters calculated for infinite clouds. The hybrid model is used for both the infinite and finite calculations. Hence, the model was accepted as displaying sufficient precision and accuracy to generate such comparisons.

5.0 THE EFFECT OF ABSORPTION ON THE CALCULATION OF DIRECTIONAL REFLECTANCE IN FINITE CLOUDS

McKee and Cox (1974), present calculations which indicate that the directional reflectance of finite clouds is substantially lower than that of infinite clouds of the same optical thickness. This effect is due mainly to cloud photons which exit the sides of the finite cloud in a downward direction. In an infinite cloud many of these photons would enter an adjacent cloud element and would have a certain probability of being scattered back in the upward direction. McKee and Cox (1974), used a scattering phase function corresponding to a wavelength of 0.45 μm with no absorption. Table 3 shows ratios of directional reflectance of finite cloud to corresponding values of infinite clouds of the same optical thickness. Values were taken from the above mentioned study. Cloud thickness and solar zenith angles are given to facilitate comparison with the results of the present study.

Cloud thicknesses (m)	0°	30°	60°
210	.74	.54	.50
630	.75	.57	.56

Table 3. Ratios of directional reflectance values, finite to infinite, from McKee and Cox (1974).

Similar values were calculated with the hybrid model with no absorption acting and the results are shown in Table 4.

Cloud thickness (m)	0°	30°	60°
210	.77	.58	.51
630	.77	.63	.58

Table 4. Ratios of directional reflectance values, finite to infinite, from present calculations with no absorption.

It can be seen that the results are similar to, although not identical with those of the previous work (McKee and Cox, 1974). In all cases the directional reflectance is smaller for finite clouds than for the corresponding infinite clouds. In addition, this effect becomes more prevalent with increasing solar zenith angle for both cloud thicknesses. The latter is merely an indication that as the sun is tipped off the zenith, more photons scatter out of the finite cloud volume through the edges of the cloud. In the finite case, for downward propagating photons, this edge effect merely allows easier escape of the photon down to the ground. In the infinite cloud this results in a higher probability that the photon will scatter upward in the adjacent cloud volume.

Table 5 shows the results corresponding to those above (Table 4) with the addition of cloud droplet absorption and water vapor absorption within the cloud. (No absorption outside the cloud volume.)

Cloud thickness (m)	0°	30°	60°
210	.85	.64	.56
630	.87	.72	.62

Table 5. Ratio of directional reflectance values, finite to infinite, in-cloud absorption included.

Although the same general features are apparent for the conservative case, the in-cloud absorption has reduced the differences in the directional reflectance values between the two types of cloud. The following explanation is offered. A photon traversing a certain path in a finite cloud will suffer the same amount of absorption as a photon traversing an identical path, in an identical volume element, of an infinite cloud. After exiting the finite cloud a photon travels to the ground or to the upper limits of the atmosphere without further depletion of energy. However, the photons which, as previously mentioned, enter the adjacent volume element of the infinite cloud (and thereby enhance the directional reflectance by being scattered in a upward direction), have their energy depeleted by additional droplet and water vapor absorptions. The net result is a convergence of directional reflectance values.

If the absorption is allowed in the atmosphere above the cloud as well as in the region surrounding the finite cloud, the results given in Table 6 are obtained.

Cloud thickness (m)	0°	30°	60°
210	.74	.55	.48
630	.78	.63	.56

Table 6. Ratios of directional reflectance values, finite to infinite, cloud and atmospheric absorption.

The results indicate that the inclusion of atmospheric, as well as in-cloud absorption, has resulted in values of the directional

reflectance ratios being similar to those of the conservative case. Part of the explanation for these results is that photons exiting the finite cloud in the upward direction now suffer absorption (by water vapor) in the atmospheric clear layer adjacent to the cloud, before reaching cloud top level. This additional absorption in the surrounding layer reduces the values of the ratios of directional reflectance from those in the previous case. Different path length distributions for upward travelling photons, after cloud exit, also influence the results. This is discussed more fully in section 6.3.

These results, which include absorption due to droplets and water vapor for the entire atmospheric and cloud photon path, are representative of a portion of the solar spectrum containing about half of the total extraterrestrial solar energy. If the results of McKee and Cox (1974), are taken as representative of the remaining half of the spectrum, where absorption is of little significance, then the conclusion that finite clouds have lower values of directional reflectance, appears to be valid for the solar spectrum as a whole.

While atmospheric plus in-cloud absorption has not changed significantly the ratios of directional reflectance of finite to infinite clouds, it has substantially reduced the values of directional reflectance themselves. For completeness, Table 7 presents all values of directional reflectance computed in this study. In considering the effect of absorption on the values of directional reflectance it should be remembered that absorption plays a significant role in the wavelength region to which these values apply. Such reductions are about twice what should be expected if directional reflectance values for the entire spectrum are being considered.

Type of Cloud	Absorption	0°	30°	60°
210 m Finite	None	.30	.25	.30
" " "	In-cloud only	.22	.19	.23
" " "	Atmosphere plus cloud	.13	.11	.12
210 m Infinite	None	.39	.43	.59
" " "	In-cloud only	.27	.29	.41
" " "	Atmosphere plus cloud	.18	.19	.24
630 m Finite	None	.53	.45	.46
" " "	In-cloud only	.35	.30	.31
" " "	Atmosphere plus cloud	.22	.18	.17
630 m Infinite	None	.69	.71	.79
" " "	In-cloud only	.40	.41	.50
" " "	Atmosphere plus cloud	.28	.29	.31

Table 7. Directional reflectance results for the 210 m and 630 m thick, finite and infinite cloud types, with varying degrees of absorption.

It is noted that although finite clouds exhibit lower values of directional reflectance than the corresponding infinite clouds, the radiant power reflected into the upper hemisphere by finite clouds can be, in some cases, greater than the radiant power reflected by an infinite cloud of the same optical thickness for an equal amount of cloud volume. This is so because a larger amount of solar radiation is received by finite clouds than the infinite cloud. For example, the ratio of directional reflectance, finite to infinite, for the 210 m thick cloud and for a solar zenith angle of 60°, is read from Table 6 to be .48, or

$$\frac{\dfrac{\text{Radiant power reflected (finite)}}{\text{Radiant power incident (finite)}}}{\dfrac{\text{Radiant power reflected (infinite)}}{\text{Radiant power incident (infinite)}}} = .48.$$

However, the ratio of radiant power incident, finite to infinite, is proportional to $(1 + \tan \theta)$, where θ is the zenith angle. So that,

$$\frac{\text{Radiant power reflected (finite)}}{\text{Radiant power reflected (infinite)}} = .48\ (1 + \tan \theta).$$

Thus, for the 60° zenith angle, this ratio becomes 1.31. Table 8 lists the ratios of reflected radiant power, finite to infinite, for cloud elements of equal volume.

Cloud thickness (m)	0°	30°	60°
210	.74	.87	1.31
630	.78	.99	1.53

Table 8. Ratio of reflected radiant power, finite to infinite, for equal volume cloud elements.

6.0 ABSORPTION OF SOLAR RADIATION IN FINITE VERSUS INFINITE CLOUDS

The theoretical considerations of the previous section indicate that the finite cloud geometry has a dramatic effect on calculated values of directional reflectance. This phenomenon is the result of photons exiting the sides of the finite cloud in the downward direction. The increased probability of photon exit from the finite cloud relative to the infinite cloud, suggests that on the average, photon optical path lengths may tend to be shorter in the finite cloud than in the corresponding infinite cloud. Since absorption of solar radiation by water vapor is crucially dependent on optical path length, and since water droplet absorption is proportional to the number of scattering encounters which increases with path length, one may hypothesize that the absorption of solar radiation in finite clouds is less than in an infinite cloud volume of the same optical thickness.

Conversely, as the sun is tipped off the zenith, the finite cloud receives more power from the sun than the corresponding volume of infinite cloud. With this information, one may argue that the absorption of solar radiation in finite clouds should be greater than in infinite clouds for other than the 0° zenith case.

Values of absorbed solar radiation calculated in this study are given in Table 9 for three layers of equal thickness in the 210 m (τ = 7.15) and 630 m (τ = 21.45) thick finite and infinite clouds and for cloud free layers of the same thickness, for zenith angles of 0°, 30° and 60°.

The results show that for the 0° zenith cases, the total absorption in the finite clouds is only a little more than half of the corresponding values in the infinite cases. As the zenith angle is increased to 30°, the finite cloud absorptions have increased to around 70% of the

Cloud Thickness (m)	Solar Zenith Angle	Cloud Layer (m above cloud base)	Absorbed Solar Radiation in watts·m^{-2}		
			Infinite	Finite	Clear
210	0°	210 - 140	16.5	12.5	4.0
		140 - 70	12.2	6.6	3.8
		70 - 0	7.7	3.0	3.7
		TOTAL	36.3	22.1	11.5
210	30°	210 - 140	14.7	11.2	3.5
		140 - 70	9.8	6.6	3.3
		70 - 0	5.8	4.5	3.2
		TOTAL	30.3	22.3	10.0
210	60°	210 - 140	8.6	6.3	2.1
		140 - 70	3.5	4.3	2.0
		70 - 0	1.8	3.8	1.9
		TOTAL	13.9	14.4	6.0
630	0°	630 - 420	47.8	31.7	11.5
		420 - 210	24.2	8.5	9.9
		210 - 0	9.9	2.1	8.9
		TOTAL	81.9	42.3	30.3
630	30°	630 - 420	39.1	28.0	10.0
		420 - 210	17.7	10.7	8.7
		210 - 0	7.2	6.0	7.7
		TOTAL	64.0	44.7	26.4
630	60°	630 - 420	14.8	14.5	5.9
		420 - 210	5.4	8.7	5.1
		210 - 0	2.3	6.3	4.5
		TOTAL	22.5	29.5	15.5

Table 9. Calculated values of absorbed solar radiation for the 210 m (τ = 7.15) and 630 m (τ = 21.45) thick finite clouds, infinite clouds and clear layers, for zenith angles of 0°, 30° and 60°.

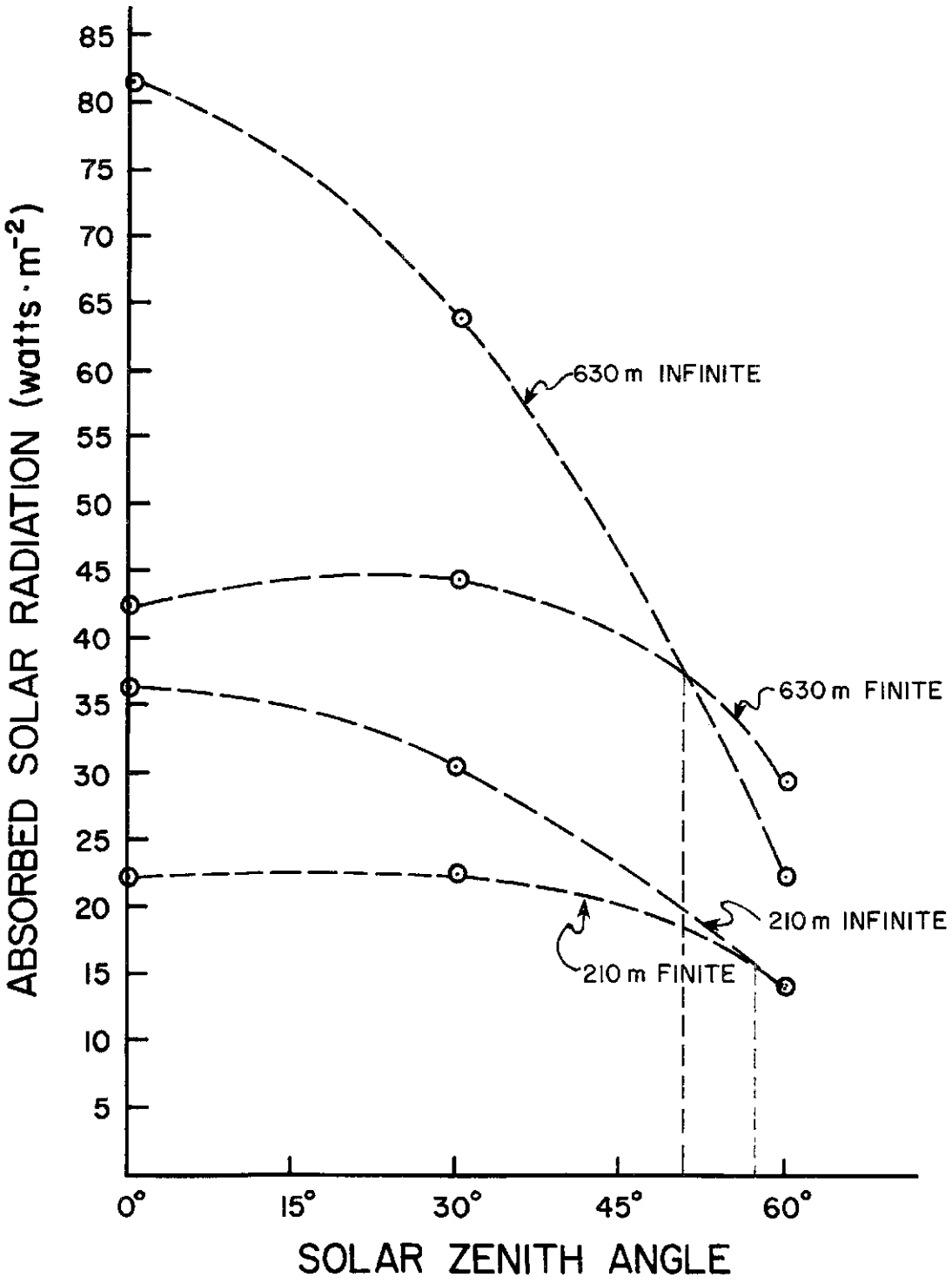

Figure 7. Absorbed solar radiation vs. solar zenith angle in the 210 m (τ = 7.15) and 630 m (τ = 21.45) finite and infinite cloud volumes.

infinite cloud values. With a 60° zenith angle the results show that the increased incidence of solar energy is dominant over the decrease in average path length, and the respective finite cloud values are 1.04 and 1.31 times as great as the values for the 210 m and 630 m thick infinite clouds. It is consistent with the above that the middle and bottom layers of the firite cloud are primarily responsible for the finite cloud's increasec absorption over that of the infinite case. These layers are exposec on one side; to direct solar radiation in the finite case, whereas in the infinite case, the two layers in question receive only the radiation which survives the encounters in the top layer and continues in a downward direction. An extreme case is seen in the bottom layer of the 630 m thick, 0° zenith, where the ratio of finite to infinite absorption is only 0.21. When the zenith angle is at 60° the same ratio increases by a factor of 13 to a value of 2.77.

Figure 7 shows a plot of the total cloud absorption values listed in Table 9. Of note is the crossover point, where the amounts of absorbed solar radiation in the two cloud geometries are equal. Although there is not sufficient data to establish the trend of the curve connecting the crossover points, it is seen that for the types of cubic, finite clouds considered here, the crossover tends to take place at lower values of the solar zenith with increasing cloud optical depth.

6.1 Horizontal distribution of solar absorption in finite clouds

The previous section compared absorption of solar radiation in finite clouds to that in equal volume elements of infinite clouds. Table 9 gave layer by layer comparisons of such values. The model also provides for the calculation of the horizontally non-homogeneous values

of absorption in the finite cloud boxes which make up the cloud layers. Figures 8 through 13 depict values for the top middle and bottom thirds of the 210 m and 630 m thick finite clouds, for zenith angles of 0°, 30° and 60°. The value to the left of the cloud boxes is the mean solar absorption in the layer, while the values in the individual boxes are adjustment factors, which when multiplied by the mean value, give the amount of solar absorption in the various boxes. All values were calculated for the in-cloud plus atmospheric absorption case and are presented unsmoothed. For more accurate values, when symmetries exist, averages should be taken to smooth the numbers. For other than the 0° solar zenith case, the solar radiation is incident on the cloud from the right hand side of the figure.

It is readily seen that the finite cloud structure has an appreciable influence on the horizontal distribution of solar absorption. In each case, cloud boxes which have the smallest probability of receiving photon energy, exhibit the lowest values of absorption. In the zero degree zenith angle case, for a given cloud layer, this probability depends only on the number of cloud box sides which are exposed to radiation, either direct or diffuse. In the 30° and 60° solar zenith angle cases, or, for boxes not in the same layer, the probability of receiving photon energy also depends, inversely, on the distance from the cloud box to the points of photon entry into the cloud. The cloud box in the center of each layer becomes relatively more important as a photon sink for the lower two cloud layers when the sun is at 0°. The opposite is true for the 30° and 60° zenith angle cases. This is caused, in the two latter cases, by the fact that it is no longer the center box which has the highest probability of receiving photon energy.

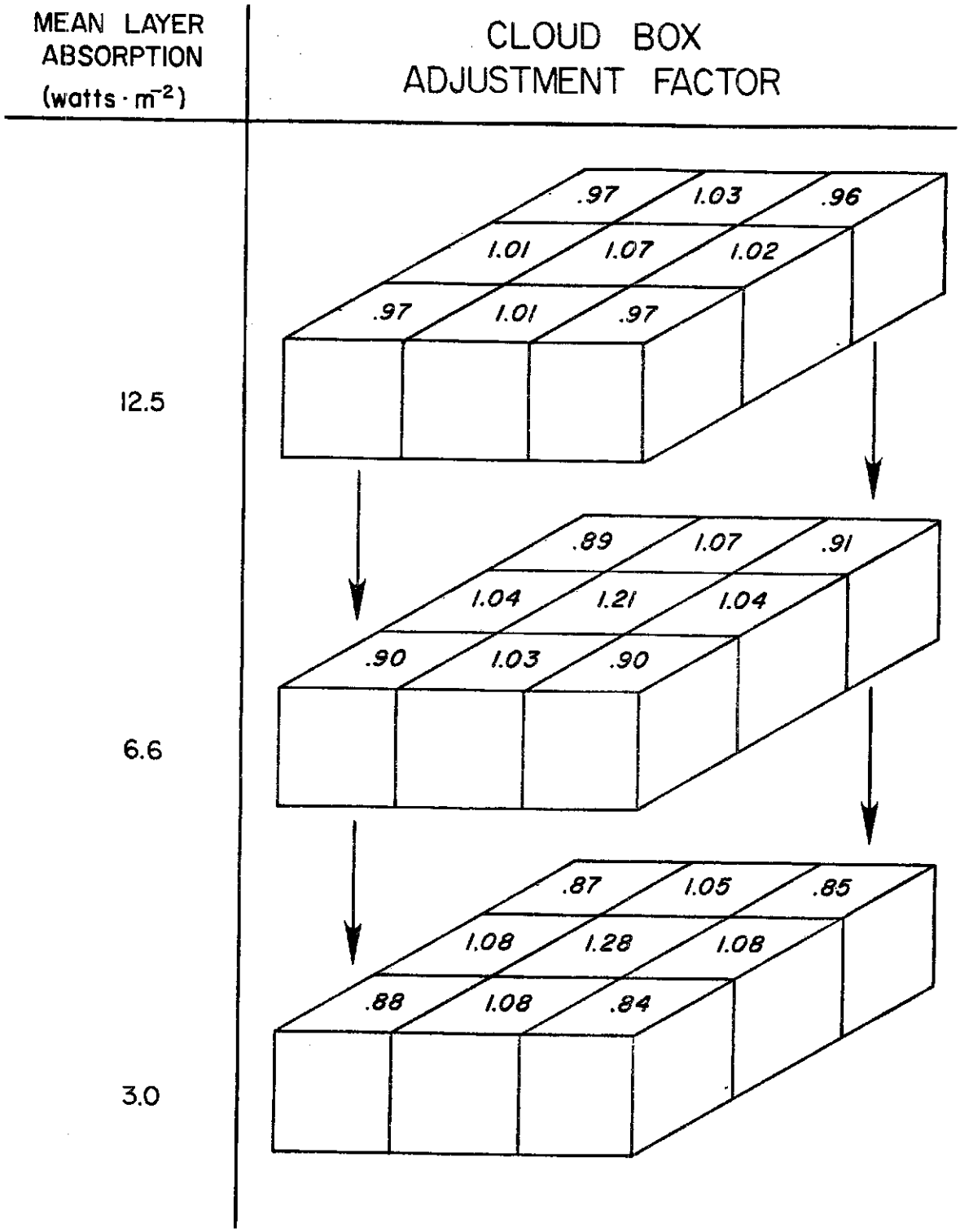

Figure 8. Mean layer solar absorptions (left) and cloud box adjustment factors (right) for the top, middle and bottom thirds of a 210 m thick finite cloud and for a solar zenith angle of 0°.

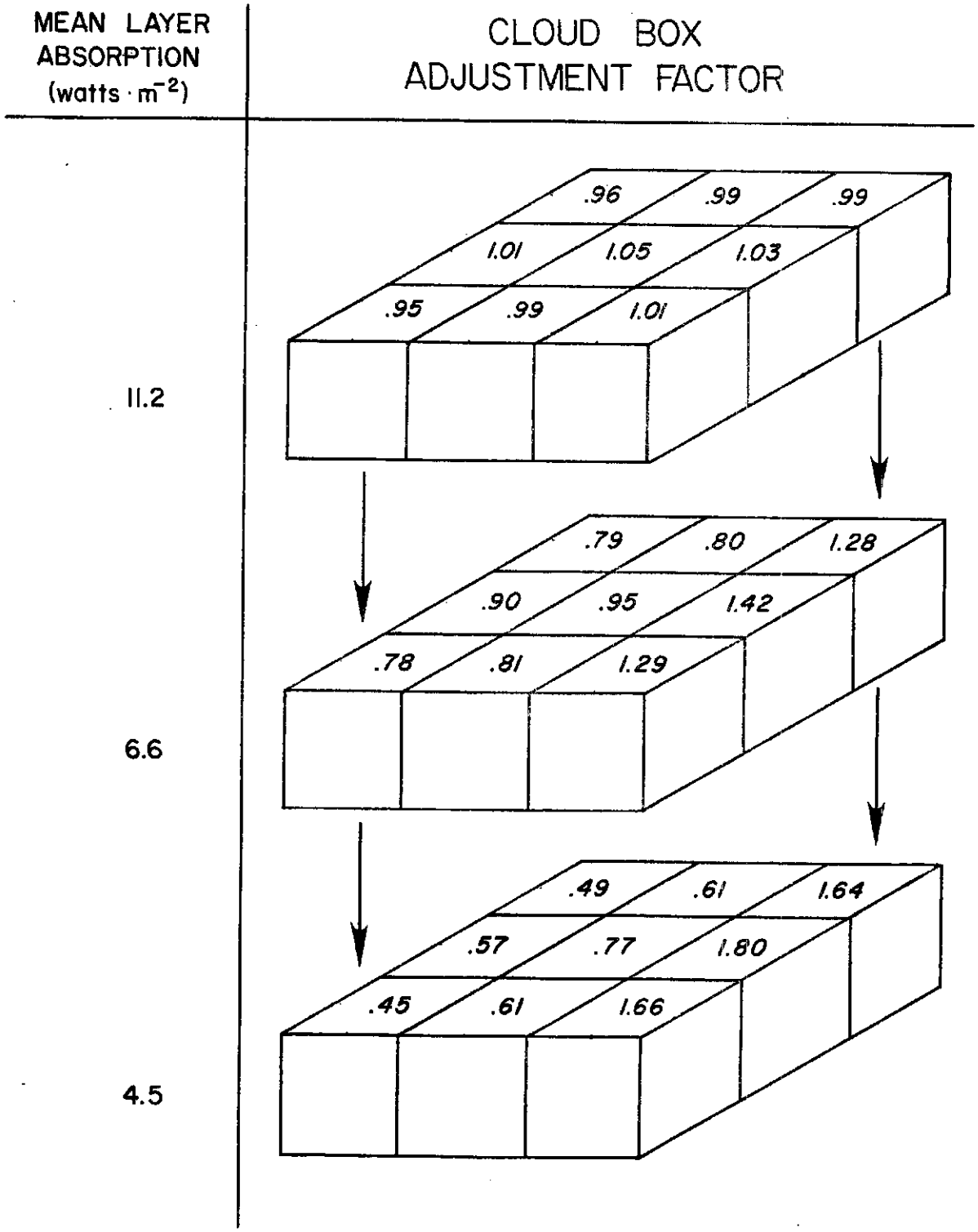

Figure 9. Mean layer solar absorptions (left) and cloud box adjustment factors (right) for the top, middle and bottom thirds of a 210 m thick finite cloud and for a solar zenith angle of 30°.

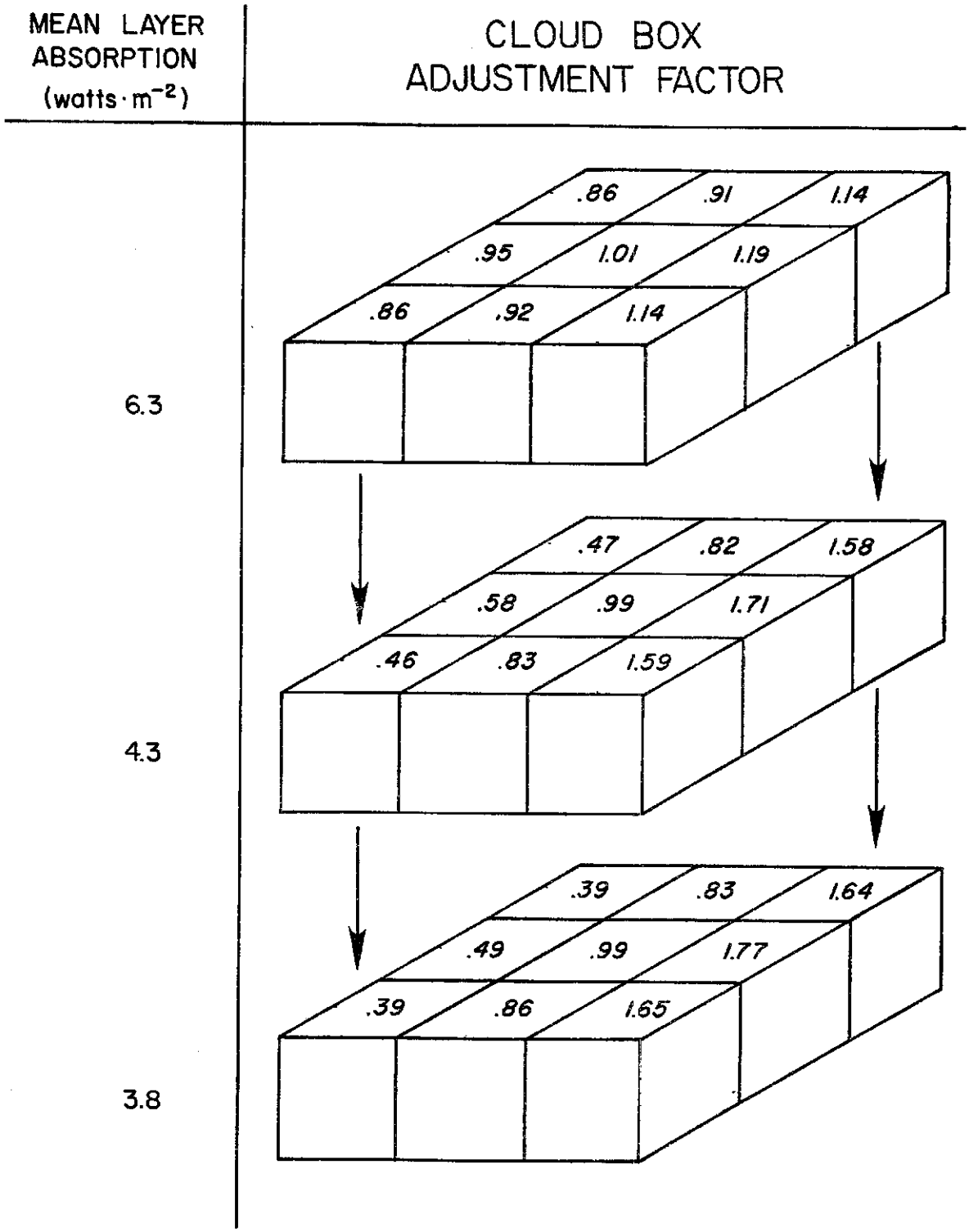

Figure 10. Mean layer solar absorptions (left) and cloud box adjustment factors (right) for the top, middle and bottom thirds of a 210 m thick finite cloud and for a solar zenith angle of 60°.

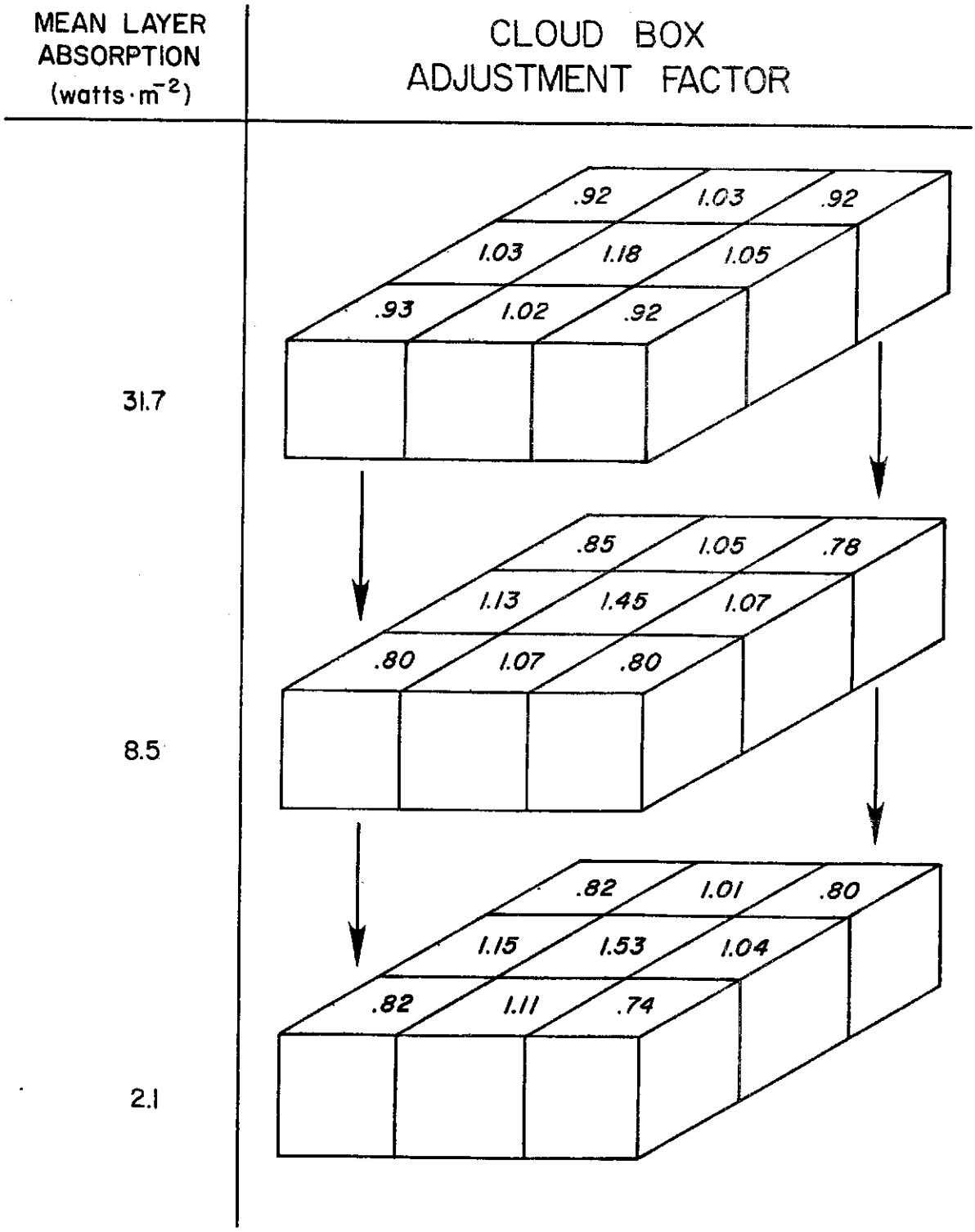

Figure 11. Mean layer solar absorptions (left) and cloud box adjustment factors (right) for the top, middle and bottom thirds of a 630 m thick finite cloud and for a solar zenith angle of 0°.

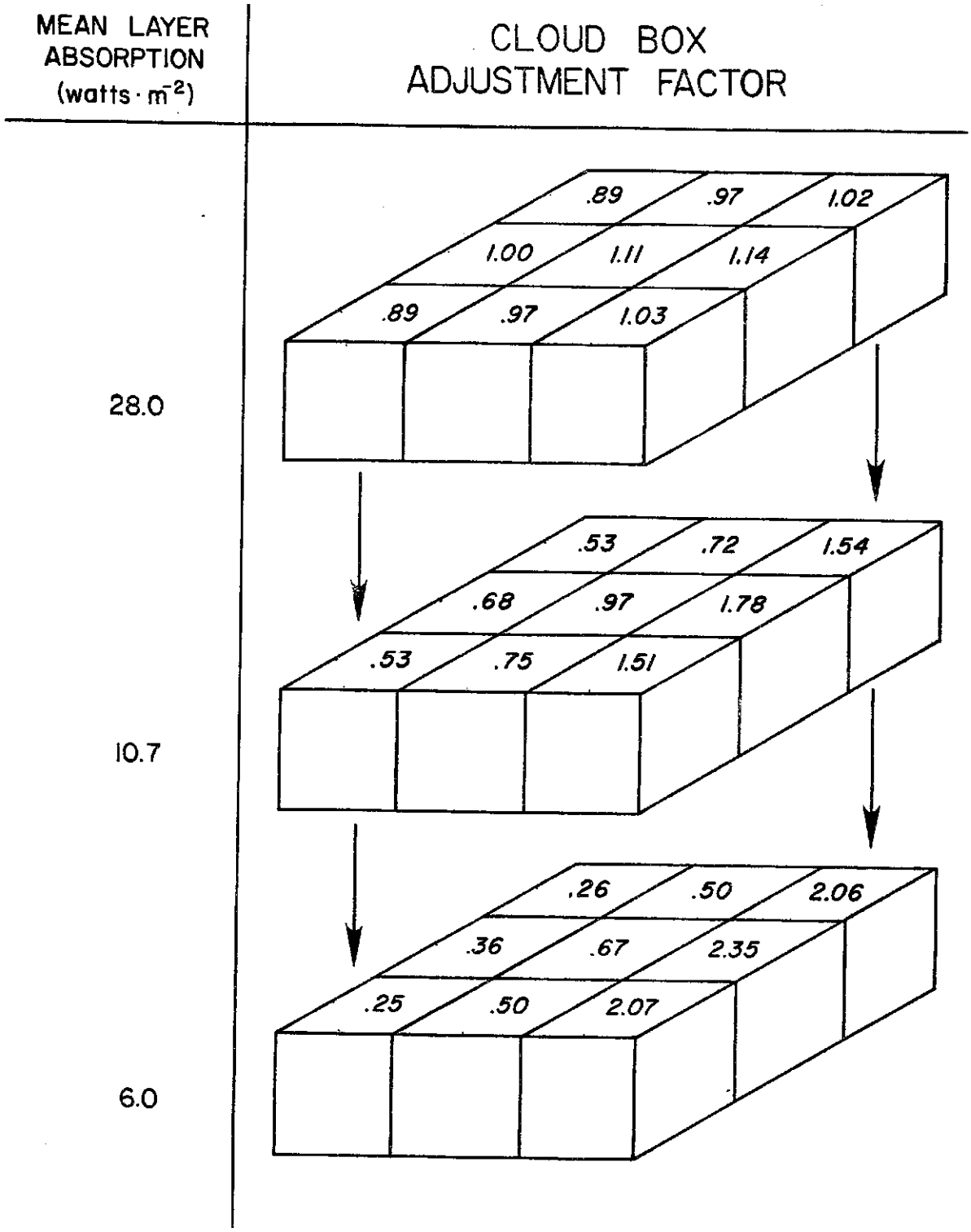

Figure 12. Mean layer solar absorptions (left) and cloud box adjustment factors (right) for the top, middle and bottom thirds of a 630 m thick finite cloud and for a solar zenith angle of 30°.

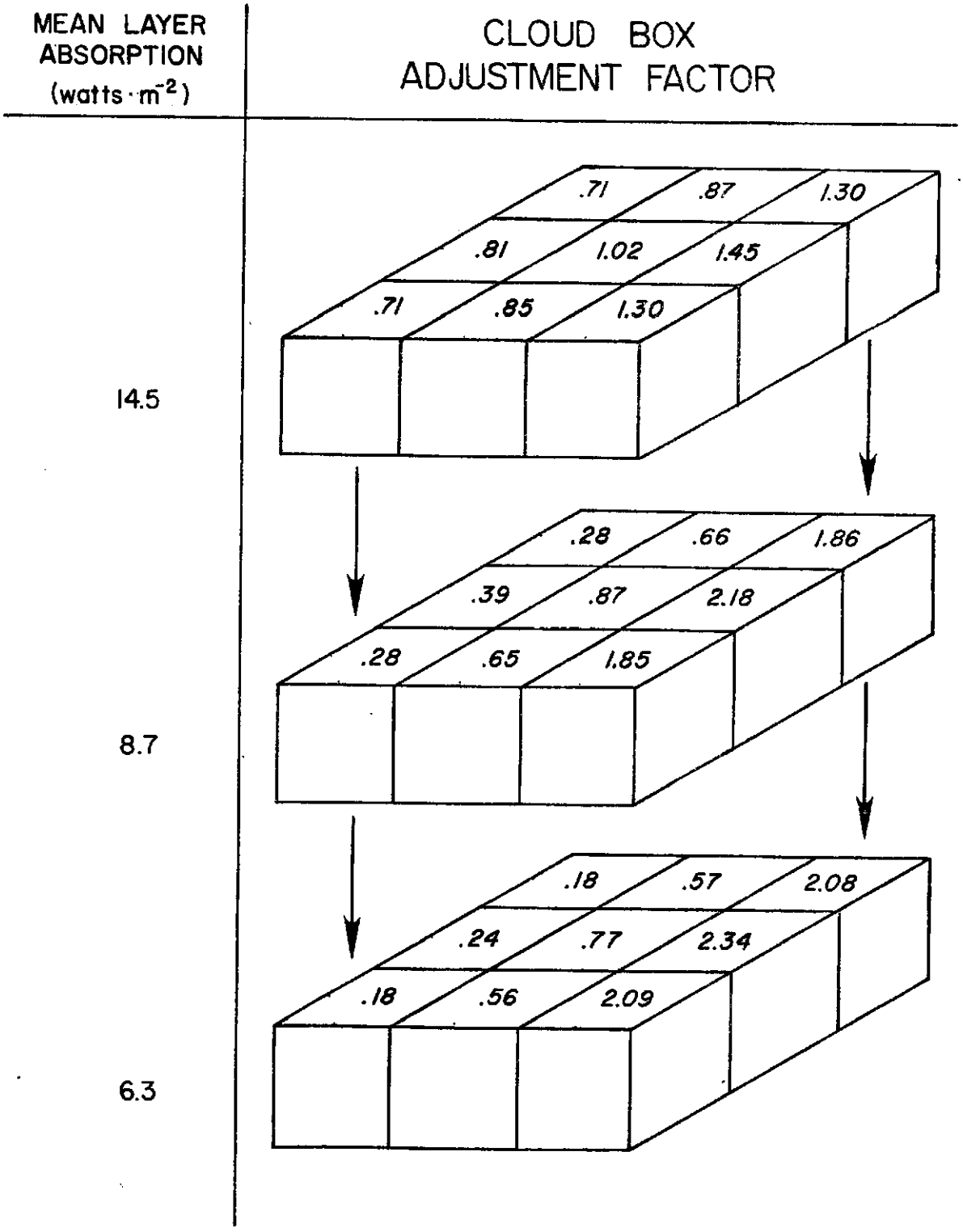

Figure 13. Mean layer solar absorptions (left) and cloud box adjustment factors (right) for the top, middle and bottom thirds of a 630 m thick finite cloud and for a solar zenith angle of 60°.

Rather, the boxes on the solar side, with one face exposed to direct radiation, receive and absorb more solar radiation relative to the other boxes in the layer.

It is interesting to note, that in the bottom layer of the 630 m cloud with a solar zenith angle of 60°, the solar absorption varies by a factor of 10 across the cloud. Perhaps more significant for purposes of this study is, that if the absorption of solar radiation were computed using the infinite cloud model, the value arrived at for the boxes on the solar side of the above layer, would be only 1/6 of the value calculated using the finite cloud model.

6.2 Absorption of solar radiation in the atmospheric region surrounding a finite cloud.

Another topic of interest which may be explored with the Monte Carlo technique is the absorption of solar radiation in the water vapor region surrounding the finite cloud. Such absorption is calculated as the loss of energy, per unit area per unit time, by photons traversing the region either before entry into the cloud or after exit from the cloud, including photons of the direct solar beam. These values were not originally envisioned as an important part of the study but are presented here because of the significant variation of absorption in the regions on the solar and anti-solar sides of the cloud. The cases considered are the same 210 m and 630 m cubic clouds, for solar zenith angles of 0°, 30°, and 60°. The calculations included the effects of atmospheric water vapor absorption above the cloud. Figs. 14 to 16 present the values of absorption. Each box depicts a region of the atmosphere having the same dimensions as an entire cloud layer, so that the surrounding region extends two cloud widths on either side of the

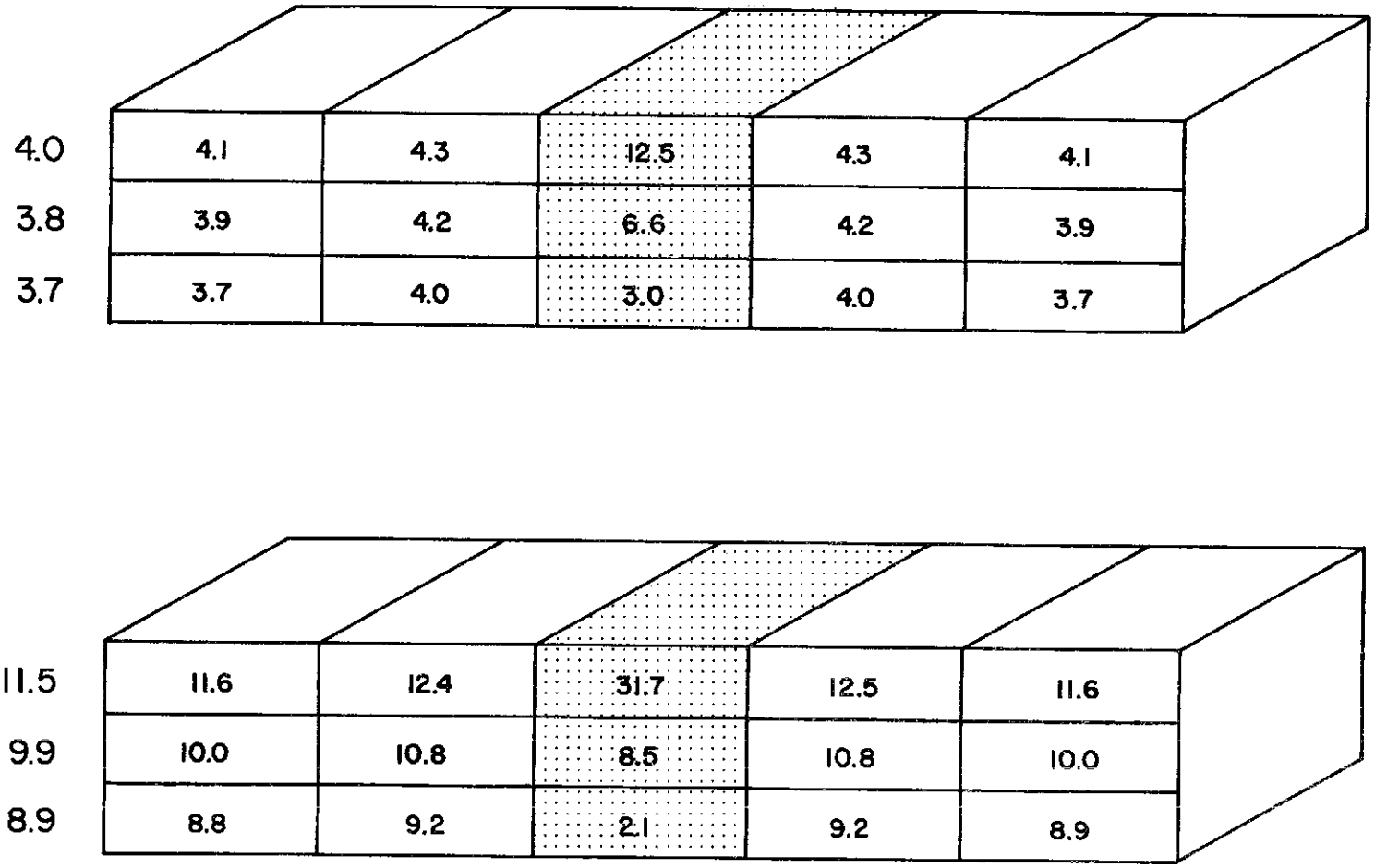

Figure 14. Solar absorption values in watts·m^{-2} for the regions surrounding the 210 m (top) and 630 m thick (bottom) finite clouds for a 0° zenith angle. Also given are cloud free layer values (left) and in cloud layer values (center).

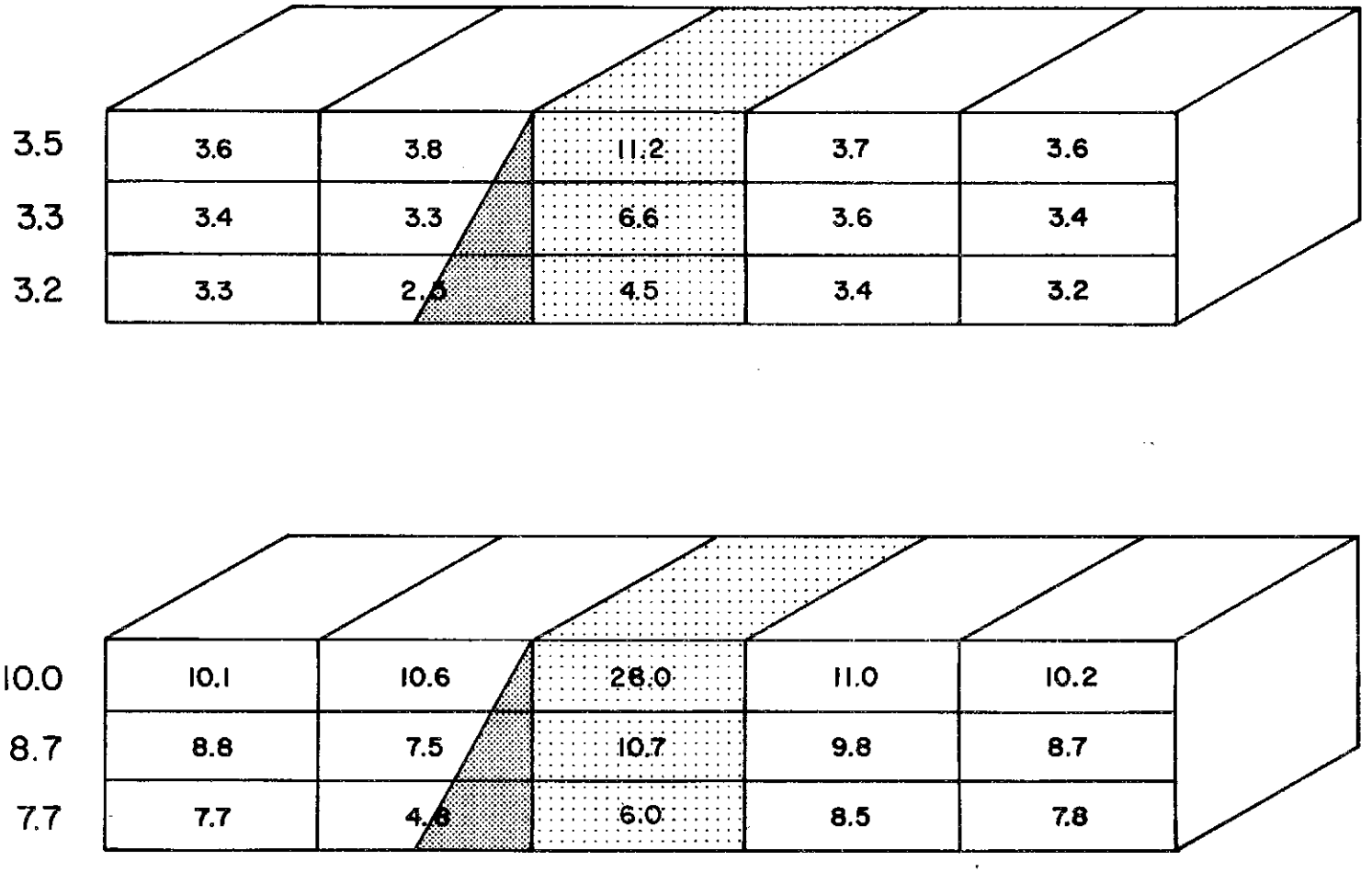

Figure 15. Solar absorption values in watts·m^{-2} for the regions surrounding the 210 m (top) and 630 m thick (bottom) finite clouds for a 30° zenith angle. Also given are cloud free layer values (left) and in cloud layer values (center).

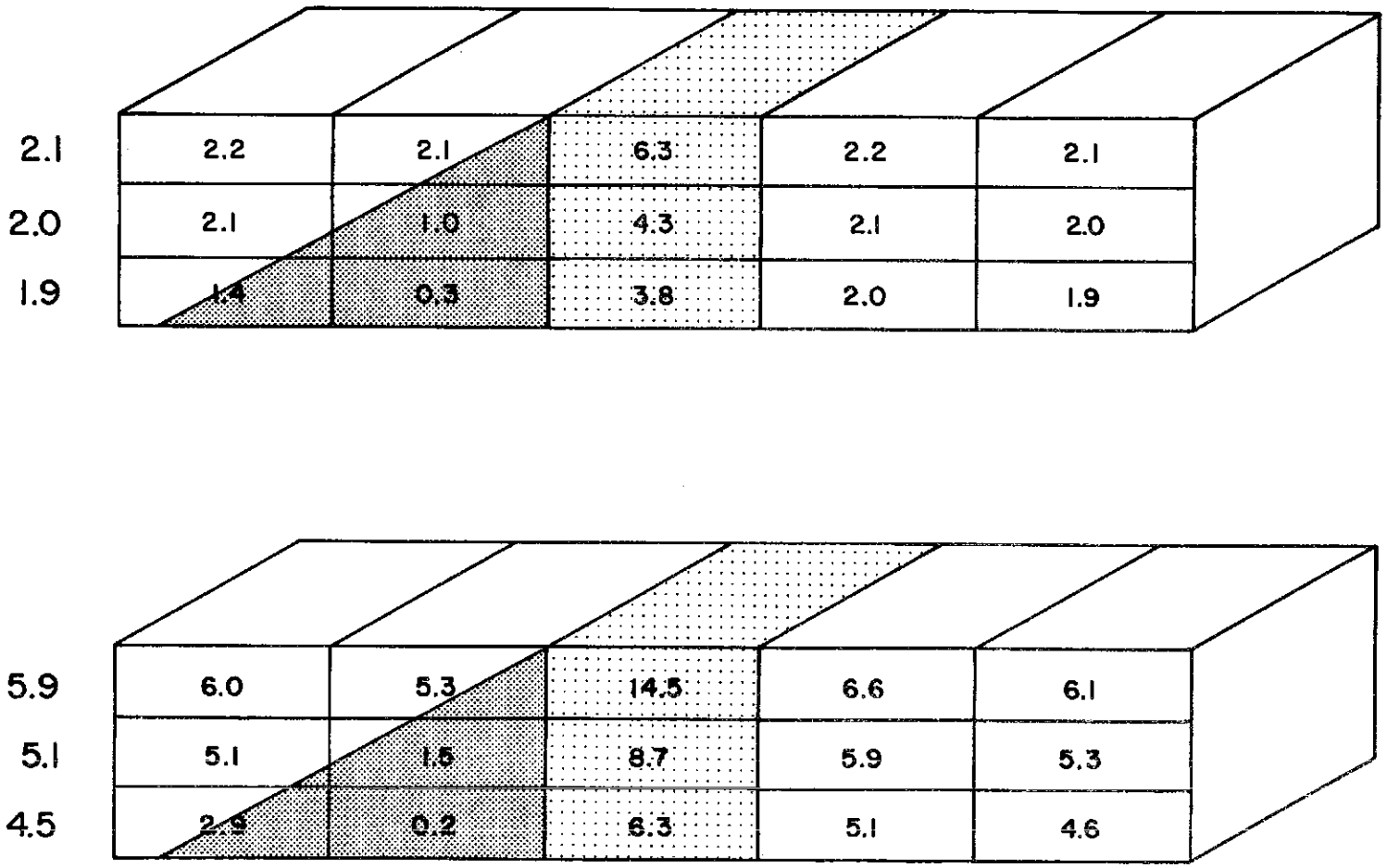

Figure 16. Solar absorption values in watts·m^{-2} for the regions surrounding the 210 m (top) and 630 m thick (bottom) finite clouds for a 60° zenith angle. Also given are cloud free layer values (left) and in cloud layer values (center).

cloud. In the 30° and 60° solar zenith angle cases, the sun's rays approach the region from the right hand side of the figure. Also depicted is the line of the geometric cloud shadow on the anti-solar side of the cloud. The absorption in a clear atmospheric layer without the influence of the cloud is given at the left of each layer. Also, the mean cloud layer absorptions are repeated here for the reader's convenience.

In the 0° solar zenith cases the effects of photons scattered from the cloud are confined almost totally to one cloud width on the solar and anti-solar sides. The 210 m cloud case does show slight absorption due to scattered photons in the most distant boxes. Similar results hold in the 30° solar zenith cases where, again, the 210 m case shows higher values than the "no cloud" values in the most distant boxes. The most distant boxes in the 630 m cloud case are virtually unaffected by scattered photons, which gives an indication of the increased optical paths (compared with those in the 210 m structure) to these boxes from the points of photon entry into the cloud. For the 60° solar zenith case both the 210 m and 630 m cloud surroundings show the effect of the scattering of the photons to the most distant boxes. This is attributed mainly to the increased number of photons scattered into the surrounding boxes. This increase in number, especially of reflected photons from the 630 m thick cloud, more than compensates for the longer paths taken in the larger cloud surroundings.

The boxes adjacent to the clouds on the solar side show moderately higher values of absorption than would be expected if the cloud were absent. This is expected because of the reflection of photons from the

solar side of the clouds. Also expected are the lower values of absorption indicated in the geometric shadows of the clouds, (see Figs. 15-16).

6.3 Absorption of solar radiation in the atmosphere above and below finite and infinite clouds.

Just as differences exist between the amounts of solar radiation absorbed in infinite clouds compared to the corresponding amounts in the finite cloud cases, there is also reason to expect differences in the absorption values above and below the different cloud elements. The calculated absorptions above the cloud result from photons traversing the water vapor in the atmosphere above the cloud before entering and also after being scattered into the upward hemisphere by the cloud. Below the cloud, absorption is due only to photons which have been scattered by or passed directly through the cloud into the downward hemisphere. Although in either case the actual absorption takes place in a large region of the atmosphere above or below the finite cloud, the present calculations were carried out as if all the absorption takes place in the volume of the atmosphere above or below the cloud, which contains the paths of the parallel radiation striking the cloud. This is done in order to permit weighting the values for the regions above or below the finite case by the amount of the adjusted fractional area of cloud cover, and combining this value with the values from clear sky calculations (weighted by the complementary fraction) to obtain an estimate for the absorption above or below a cloud field. The adjusted fractional cloud cover area referred to can be calculated as the product of the geometric fractional cloud cover area and the quantity $(1 + \tan \theta)$, where θ is the solar zenith angle (see

Fig. 18 and Section 8.5). Table 10 lists the calculated absorption values for regions above the 210 m (τ = 7.15) and 630 m (τ = 21.45) thick clouds for solar zenith angles of 0°, 30° and 60°. Also given are corresponding values for the regions above the infinite cloud and above the no cloud case. It should be remembered that the cloud volume elements are immersed in a tropical atmosphere and that cloud top is at 1.5 km in both cases.

Cloud Thickness (m)	Solar Zenith Angle	Absorbed solar radiation above cloud top in watts·m^{-2}		
		Infinite	Finite	No Cloud
210	0°	292	293	272
210	30°	264	259	244
210	60°	170	169	160
630	0°	299	302	272
630	30°	269	265	244
630	60°	174	170	160

Table 10. Values of absorbed solar radiation above the 210 m (τ = 7.15) and 630 m (τ = 21.45) thick finite and infinite clouds, and for a corresponding region with no underlying clouds.

The values in Table 10 may be used directly to obtain heating rates for the respective volume elements. Note that the cloud elements are of equal volumes but the regions above the cloud elements, to which the values in Table 10 refer, are not of equal volume. The region above the finite cloud has a volume which is larger by the factor (1 + tan θ) [see Fig. 18].

To more closely examine the absorption of the reflected radiation one must remove the absorption due to the parallel beam on its way down to the cloud, see Table 11, which also gives the associated values of the reflected radiant power absorbed above the clouds. These values eliminate the effects of the different surface areas being considered above the finite and infinite clouds.

Cloud Thickness (m)	Solar Zenith Angle	Absorption of reflected radiation only (watts·m^{-2})		Corresponding radiant power (megawatts)	
		Infinite	Finite	Infinite	Finite
210	0°	20	21	.9	.9
210	30°	20	15	.9	1.0
210	60°	10	9	.4	1.0
630	0°	27	30	10.7	11.9
630	30°	25	21	9.92	13.1
630	60°	14	10	5.56	10.8

Table 11. Absorption of reflected radiation and corresponding amounts of reflected radiant power.

The results indicate that the amount of radiant power absorbed above the finite cloud is in every case greater than or equal to that absorbed above the infinite cloud. An analysis of the results in Table 5 makes these findings somewhat more credible. Table 5 gives ratios of directional reflectance, finite to infinite, for the case of absorption in the cloud elements only. Although these ratios do not include absorption of photons on the way down to the cloud elements, which should be essentially the same in both cases, the values do suggest

that, in all but the 0° solar zenith angle cases, finite clouds scatter more radiant power into the upper hemisphere than the corresponding infinite elements. (The finite clouds receive [1 + tan θ] more radiant power than the infinite volume elements). The higher absorption values at 0° zenith indicates that photons which exit the finite cloud in the upward hemisphere have a greater chance of doing so at larger angles, with respect to the vertical, than do the photons which exit the infinite cloud. In this way such photons traverse a relatively larger optical path, especially in the first few layers above cloud top. For example, Figure 17 shows frequency histograms of the angle of exit from the cloud for photons travelling in the upward direction for the 210 m, 0° zenith angle finite and infinite clouds. Such behavior is also consistent with the changes in the directional reflectance ratios, seen by comparing the values of Table 5 with those of Table 6.

The amounts of solar radiation absorbed below the cloud structure are presented in Table 12. Again in the finite case, the absorption has been calculated as if it were confined to a volume which is the atmospheric column of the geometric cloud shadow. For cloud elements of the same volume this region is again larger beneath the finite cloud than the volume below the infinite element by a factor of (1 + tan θ). Cloud base for the 210 m and 630 m thick clouds are at 1.29 km and at 0.87 km respectively.

In view of the previous results and discussion, which referred to the relative amounts of radiant power received by the different cloud geometries, it is expected that absorption below the finite cloud exceeds that below infinite cloud in the 30° and 60° solar zenith angle cases. Because of the increased probability of photons being scattered

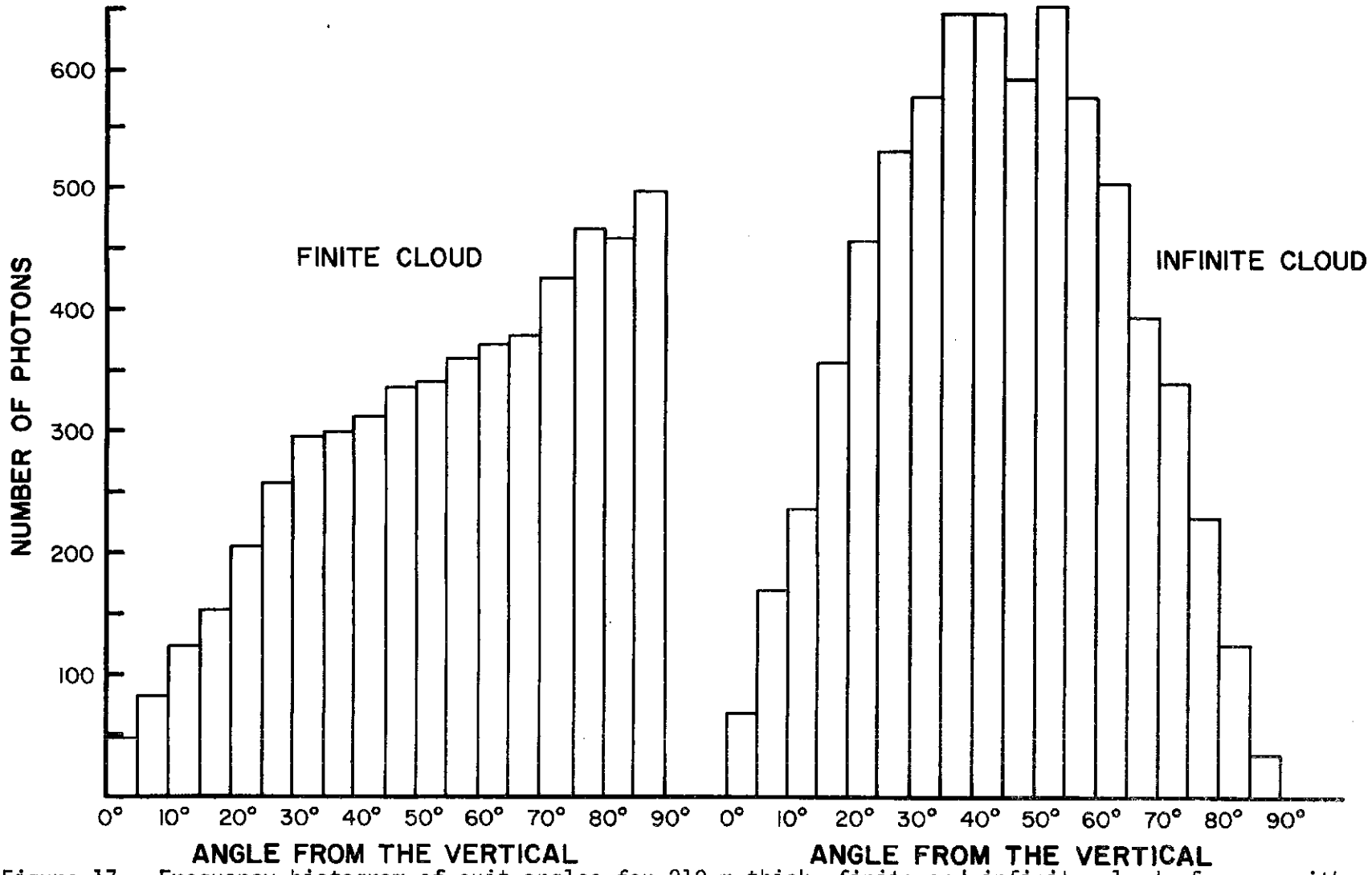

Figure 17. Frequency histogram of exit angles for 210 m thick, finite and infinite clouds for a zenith angle of zero degrees.

Cloud Thickness (m)	Solar Zenith Angle	Absorbed solar radiation below cloud base in watts·m^{-2}		
		Infinite	Finite	No Cloud
210	0°	31.7	44.3	48.1
210	30°	23.5	38.0	41.8
210	60°	7.1	18.2	24.4
630	0°	7.1	19.3	30.6
630	30°	4.33	18.4	26.6
630	60°	1.73	8.8	15.5

Table 12. Absorption of solar radiation in the atmospheric layers below the 210 m and 630 m thick, finite and infinite cloud elements and also for the corresponding cloud free case.

from the sides of the finite cloud in the downward direction, it is consistent that this is also true in the 0° zenith angle case. Perhaps the most significant result in the table is that for the thin 210 m (τ = 7.15) finite cloud, absorption below the cloud is almost 75% of the value in the no-cloud case. Even for the thicker 630 m (τ = 21.45) thick finite cloud these values remain over 50% of the cloud free amounts.

7.0 SOLAR IRRADIANCE AT THE SURFACE BENEATH THE FINITE AND INFINITE CLOUDS

The final but perhaps one of the most important radiative parameters which is examined in this research is the amount of solar irradiance which reaches the earth's surface beneath the finite and infinite cloud volumes. The surface temperature of the earth, which is greatly influenced by the amount of solar irradiance incident at the ground, is crucial in controlling the exchange of water vapor and sensible heat between the earth's surface and the boundary layer. Large discrepancies between values of solar irradiance at the earth's surface, calculated by the finite vs. infinite cloud models, should be taken into account in any attempt to model the boundary layer.

In the last few sections of Chapter 6, values of absorbed solar radiation above or below the finite cloud case were calculated as if the absorption was confined to a volume element larger than that corresponding to the infinite cloud volumes by the factor $(1 + \tan \theta)$, where θ is the solar zenith angle. This same procedure is used to present the solar irradiance at the earth's surface. The reason for adopting this method of presentation becomes apparent, especially when considering this last of the calculated parameters. If one attempts to estimate the differences in solar irradiance at the surface, for a field of clouds, using finite cloud calculations instead of infinite cloud calculations, it is necessary to weight the calculated values in some fashion, according to the amount of area cloud cover. When employing values of surface solar irradiance calculated by the infinite cloud model, it is normal to simply weight these results by the fractional amount of cloud cover and combine these numbers with clear sky values

weighted by a complementary fraction. However, the hypothetical, cubic, finite cloud used in this model will intercept a larger fraction of the parallel solar beam than the equal volume element in an infinite cloud calculation for other than a 0° zenith angle. When attempting to weight the values of irradiance at the surface calculated by the finite model, it must be remembered that the amount of surface area which is in the geometric shadow of the cloud volume is larger than the amount assigned to an equal volume of infinite cloud. Thus, when calculating the ratio of cloud to clear area, which should be used for cloud field calculations using the finite cloud model, the fractional area of finite cloud cover should be multiplied by the factor $(1 + \tan \theta)$. Figure 18 illustrates the geometry for the two types of weighting for a solar zenith angle of θ degrees. Obviously such a weighting scheme can be employed for fractional area cloud covers less than or equal to $1/(1 + \tan \theta)$. For larger amounts of cloud cover one could assume 100% cloud cover when using the finite values. However, in such a case, it is likely that the reflected radiation from one cloud which interacts with neighboring clouds would become important. Since such interaction has not been incorporated into this model, such applications would be questionable here. The results shown in Table 13 indicate that the values calculated by the finite cloud model are significantly different than those which would be derived from an infinite cloud calculation. The relative differences increase with zenith angle for a given optical depth and also increase with optical depth for a given zenith angle, at least for the values of such parameters employed in this study.

Although the results of Chapter 6 may be accepted as representative of the entire solar spectrum (because nearly all absorption takes place

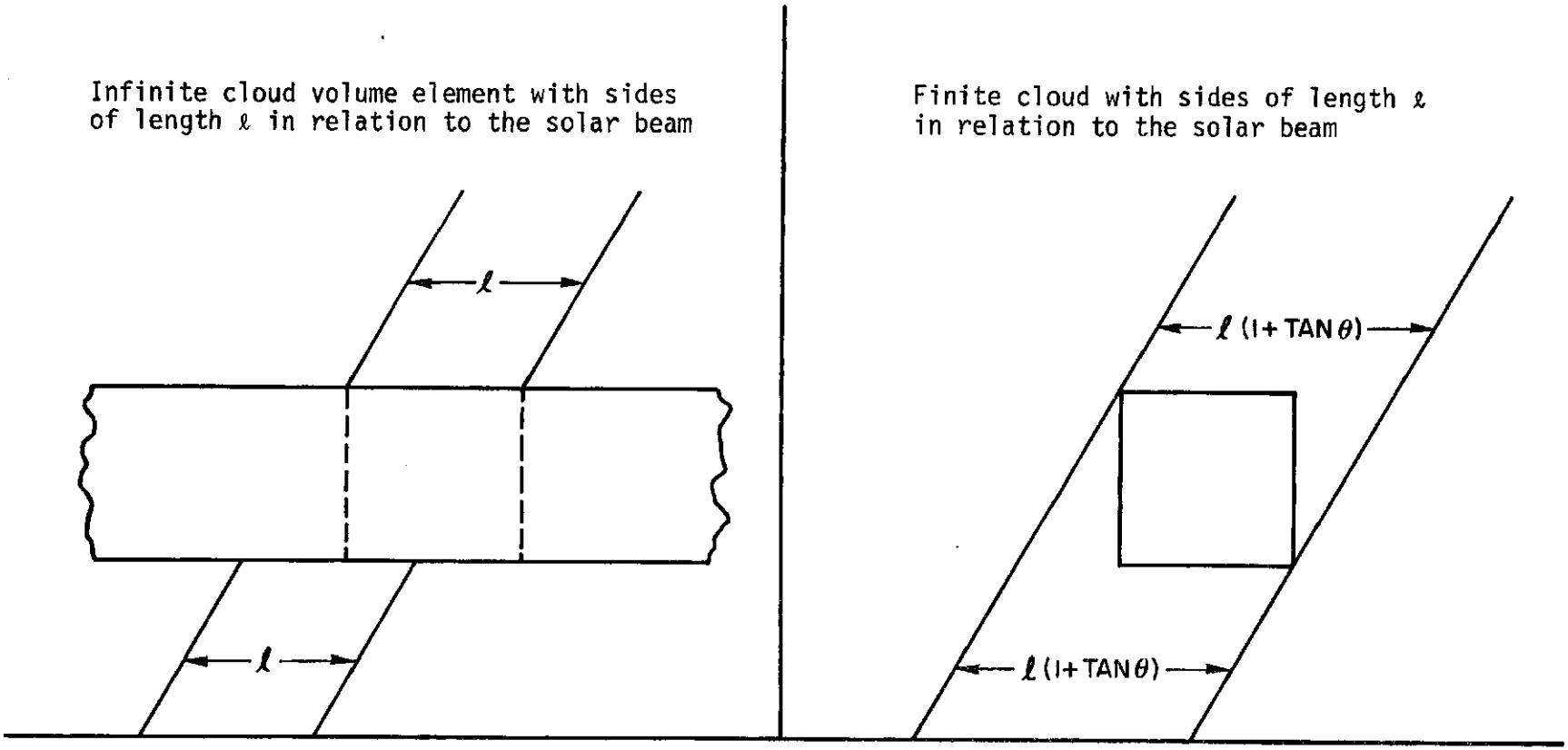

Figure 18. Geometry depicting the amounts of weighting which should be used in cloud field calculations using the infinite and finite cloud models.

Cloud Thickness (m)	Solar Zenith Angle	Solar irradiance at the earth's surface in watts·m^{-2}		
		Infinite	Finite	No Cloud
210	0°	175.8	196.0	316.0
210	30°	137.4	182.1	266.4
210	60°	54.1	88.6	134.3
630	0°	76.0	123.5	316.0
630	30°	59.6	127.0	266.4
630	60°	24.8	66.9	134.3

Table 13. Solar irradiance at the earth's surface for the 210 m (τ = 7.15) and 630 m (τ = 21.45) thick, finite and infinite cloud elements and also for the cloud free case.

within the wavelength region being studied), the results of Table 13 cannot. In addition to the solar irradiance at the surface which is calculated in this study, one must account for the solar irradiance striking the ground in the shortwave portion of the spectrum from 0.3 microns to 0.8 microns. The latter is depleted on its way to the ground by droplet scattering as well as by Rayleigh scattering. An approximation of the amount of solar irradiance at the surface, in this part of the spectrum, can be made utilizing the directional reflectance values as presented in McKee and Cox (1974), which are applicable at a wavelength of 0.45 microns. In the approximation of this part of the spectrum, absorption is neglected since it is small and Rayleigh scattering is assumed to scatter 8% of the total extra-terrestrial solar radiation back in the upward direction. Combining this approximation with the values of Table 13 results in values of solar irradiance at the earth's surface for the entire solar spectrum as shown in Table 14.

The results of Table 14 indicate that including an approximation for the remainder of the solar spectrum does not change the relationships between the values of surface solar irradiance calculated by the finite and infinite cloud models.

Cloud Thickness (m)	Solar Zenith Angle	Solar irradiance at the earth's surface (entire solar spectrum) in watts·m^{-2}		
		Infinite	Finite	No Cloud
210	0°	605.4	675.1	932.8
210	30°	485.5	616.8	800.7
210	60°	208.9	321.2	443.2
630	0°	317.7	460.7	932.8
630	30°	250.1	464.3	800.7
630	60°	107.8	250.9	443.2

Table 14. Solar irradiance at the earth's surface for the 210 m (τ = 7.15) and 630 m (τ = 21.45) thick, finite and infinite cloud elements estimated for the entire solar spectrum.

8.0 IMPLICATIONS OF THE RESULTS

The preceeding chapters have indicated that the hybrid model used in this study predicts values of directional reflectance, absorbed solar radiation and surface solar irradiance which are substantially different for finite clouds than analogous values calculated for infinite clouds. The present chapter is an attempt to demonstrate what effects such findings may have on certain topics within the atmospheric sciences.

8.1 The effect of finite cloud results on albedo calculations

One of the most obvious applications of the directional reflectance results is the calculation of the earth's albedo. Since finite clouds have been shown (see Section 5.0) to reflect different amounts of energy compared to infinite clouds, albedos estimated by infinite cloud calculations will not yield the same results as those calculated from the finite cloud model. Although such calculations are complex, requiring detailed knowledge of types and amounts of cloud cover, surface characteristics and cloud scattering features, a simple calculation showing the importance of the finite geometry on areal directional reflectances can be made. The directional reflectance of the region can be defined as the radiant power reflected into the upward hemisphere by a certain area of the earth-atmosphere system divided by the direct solar radiant power incident on the area. In order to obtain directional reflectance values representative of the clouds (assumed to be finite) of the region, the directional reflectance values from McKee and Cox (1974), are employed for wavelengths below 0.7 μm. These values are combined with the results of the present research, which represent wavelengths from 0.7 to 8.0 μm, according to the amount of extra-terrestrial

radiant power in each wavelength region. The clouds are assumed to exist above a totally absorbing surface and a simple weighting calculation is used to obtain the areal directional reflectance values. The ratios, finite to infinite, of areal direction reflectances are 0.74, 0.86 and 1.34 for 0°, 30° and 60° zenith angles in the 210 m thick (τ = 7.15) case. Analogous ratios for the 630 m thick (τ = 21.45) cloud are .76, .92 and 1.52 for the solar zenith angles of 0°, 30° and 60°. These ratios simply demonstrate the enhanced downward scattering characteristics of the finite cloud at small zenith angles to decrease the ratio and the increased receipt of radiant power by the finite cloud for larger zenith angles to increase the directional reflectance of the finite cloud above that of the infinite cloud volume. If the clear atmosphere is assumed to make a non-zero contribution to the directional reflectance, the calculated ratios, finite to infinite, are no longer constants but vary with amount of cloud cover. Figures 19 and 20 show the results of such a calculation in which the clear portion of the atmosphere is assumed to contribute a directional reflectance of 5% to the weighting scheme. The directional reflectance values of the finite clouds are multiplied by the factor (1 + tan θ) in the calculations in order to account for the greater amount of incident radiant power in the finite cloud case. The ratios of directional reflectance are plotted as a function of area cloud cover up to the point at which the surface would receive no direct solar radiation in the finite cloud case.

The results indicate that areal directional reflectance values are zenith angle dependent. At zenith angles of 60°, the increased receipt of solar radiation is dominant over the decreased values of directional reflectance in the finite clouds and the calculated ratios are

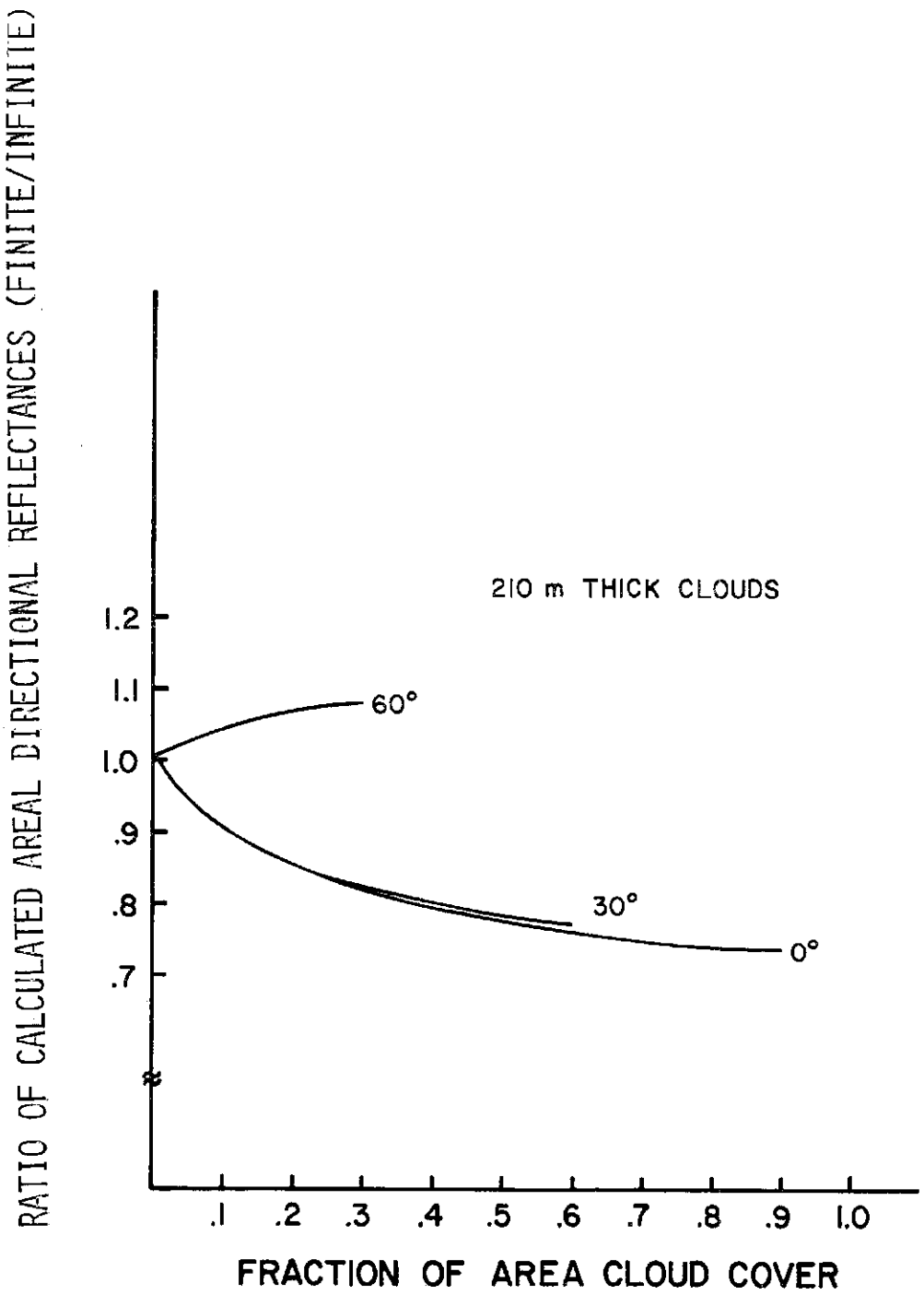

Figure 19. Ratios of calculated areal directional reflectances, finite to infinite, vs. fractional area cloud cover for the 210 m thick cloud (τ = 7.15) and solar zenith angles of 0°, 30° and 60°.

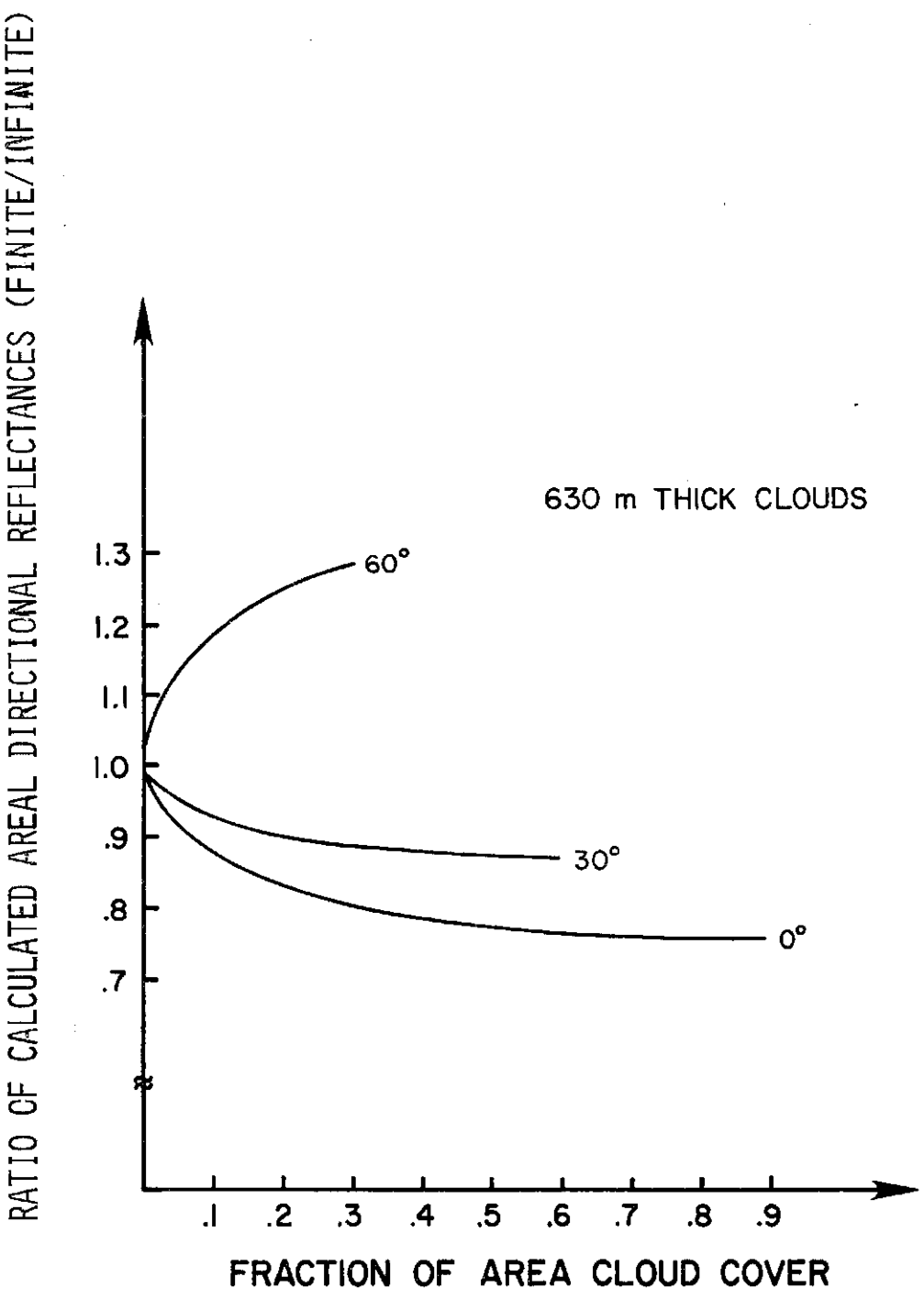

Figure 20. Ratios of calculated areal directional reflectances, finite to infinite, vs. fractional area cloud cover for the 630 m thick cloud (τ = 21.45) and solar zenith angles of 0°, 30° and 60°.

correspondingly higher. Although calculations of areal directional reflectance in the manner described above are an extreme simplification of the problem, they represent first order approximations, and as such indicate that resulting values calculated over cloud fields may be significantly in error if finite scattering properties are ignored.

Also, if measured directional reflectance values are used to infer various other atmospheric properties such as cloud thickness, cloud height or amount of area cloud cover, then similar errors may result if finite cloud scattering properties are ignored.

It is noted that the calculated ratios are also highly dependent on the directional reflectance value assigned to clear regions. For example, if the clear region is assigned a directional reflectance value of 0.20, then at 30% cloud cover the calculated ratio in the 630 m thick cloud for 60° zenith angle is .923.

8.2 The effect of finite cloud calculations on estimates of surface solar irradiance

Chapter 7 compared values of surface irradiance beneath the finite and infinite cloud volume elements. Using the values listed in Table 14 a simple approximation may be made for the solar irradiance at the surface beneath a broken cloud field. To stress the importance of the finite cloud geometry, the same calculation is compared to one using the infinite cloud results. The area weighting for the different cloud geometries is the same that has been used throughout this study. Figure 21 shows plots of the ratios of mean surface solar irradiance which result from a simple calculation using the values of Table 14. The values for the 30° and 60° solar zenith angle cases have been plotted only to the point at which the adjusted fractional cloud cover equals unity.

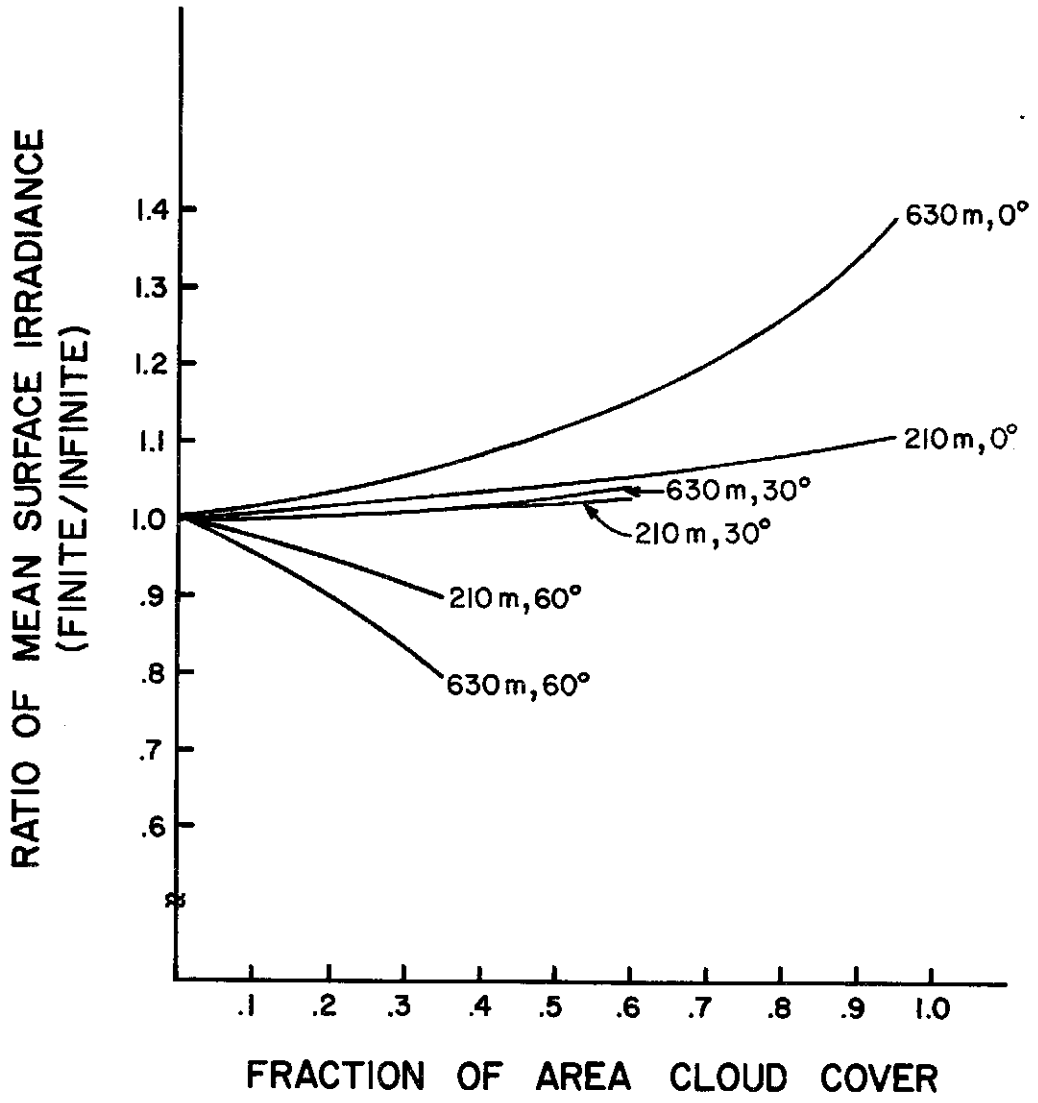

Figure 21. Ratio of estimated mean surface solar irradiance (finite/infinite), vs. fraction of area cloud cover for the 210 m (τ=7.15) and 630 m thick clouds (τ=21.45) for solar zenith angles of 0°, 30° and 60°.

As is indicated by the graph, for a fractional area cloud cover of less than 0.5, the finite and infinite calculations lead to values of mean surface solar irradiance which are within 5% of each other for the 210 m, 0° zenith case as well as the 210 m and 630 m 30° zenith cases. For this same amount of cloud cover, the 630 m, 0° zenith values differ by more than 10%. At 0.3 sky cover differences of 10% and 20% are evident in values calculated for the 210 m, 60° and the 630 m 60° cases respectively. Note that the ratios calculated for the 0° zenith angle cases are greater than unity. In these cases, since the different cloud geometries contribute identically in the weighting scheme, it is only the enhanced scattering in the downward direction which accounts for the higher irradiance values. Also it is apparent that the ratio of surface solar irradiances is zenith angle dependent. Thus, any conclusions regarding the differences existing between values of surface irradiance, beneath finite and infinite clouds, over an extended period of time, should be drawn from values which have been integrated over time.

8.3 An application of the finite cloud results to a model of the mixed layer

Many models of atmospheric processes include the energy input from solar radiation in some form or another. Modeling of the lowest layers of the earth's atmosphere in particular requires some input of the variation of solar energy into the system. One example is Lilly's cloud-topped mixed layer model which was used by Schubert (1976), to examine the properties of the mixed layer subject to a diurnally varying radiative flux. Basically the model is applied to a mixed layer capped by non-precipitating stratocumulus and trade cumulus clouds. The model assumes horizontal homogeneity and the radiative flux is entered as net

upward longwave flux minus a diurnally varying absorption of solar radiation by the cloud. Although the clouds are considered to be uniform in the horizontal, in reality stratocumulus clouds are composed of closed convective cells, therefore, such a cloud field may display certain features of the finite cloud field. In particular, if the regions between cells are less optically thick, significant amounts of radiation may enter the sides of the cells. Thus, the absorption may tend to behave as it does in finite clouds described in Chapter 6.0. The formulation of the net radiative flux is given as

$$\Delta F_{RINF} = 90.0 - 69.77 \max \left\{ \begin{matrix} .202 + .779 \cos \left(\frac{2\pi t_d}{24}\right) \\ 0 \end{matrix} \right\} \text{watts} \cdot \text{m}^{-2}$$

The first right hand side term is the net upward longwave flux, while the second term is the solar radiation absorbed by the cloud and t_d is the time of day measured in hours from local noon. The effect of the finite cloud geometry may be included by using the results of Chapter 6 concerning absorption in finite vs. infinite clouds. First, the ratio of absorptions in the 630 m thick cloud, finite to infinite is plotted versus zenith angle, and zenith angles are calculated as a function of t_d for a particular day number. Secondly, the ratio plot is fitted to the time of day and this factor is then used to multiply the second term in the radiative flux expression. Such a procedure carried out for day 200 results in the following expression

$$\Delta F_{RFIN} = 90.0 - 69.77 \max\left\{ \begin{matrix} .202 + .779 \cos\left(\frac{2\pi t_d}{24}\right) \\ 0 \end{matrix} \right\} \cdot \left\{ .584 \left(\frac{2\pi t_d}{24}\right)^2 + .525 \right\} \text{watts} \cdot m^{-2}.$$

Figure 22 shows a plot of ΔF_{RFIN} and ΔF_{RINF}. Since fluxes of water vapor plus liquid water and moist static energy are highly correlated with the radiative flux, significant variation in these fluxes may result if finite absorption characteristics were included. Thus, modeling of the mixed layer may be significantly affected. For example, Figure 23 shows the effect of including finite cloud properties on the thickness of the stratus layer and on the product of the latent heat of evaporation times the flux of liquid water plus vapor just below the top of the mixed layer. Although the diurnal variation of the thickness of the stratus deck is not greatly affected, the model does indicate that the diurnal variation of the flux of liquid water and water vapor is significantly changed. The dashed line in the bottom part of Fig. 23 is an upper limit of the finite cloud effects in such a model since the curve was derived from incorporation of the absorptive properties of an isolated finite cloud into the mixed layer model. Typical curves for a cellular stratus deck would lie between the solid and dashed curves shown in Fig. 23.

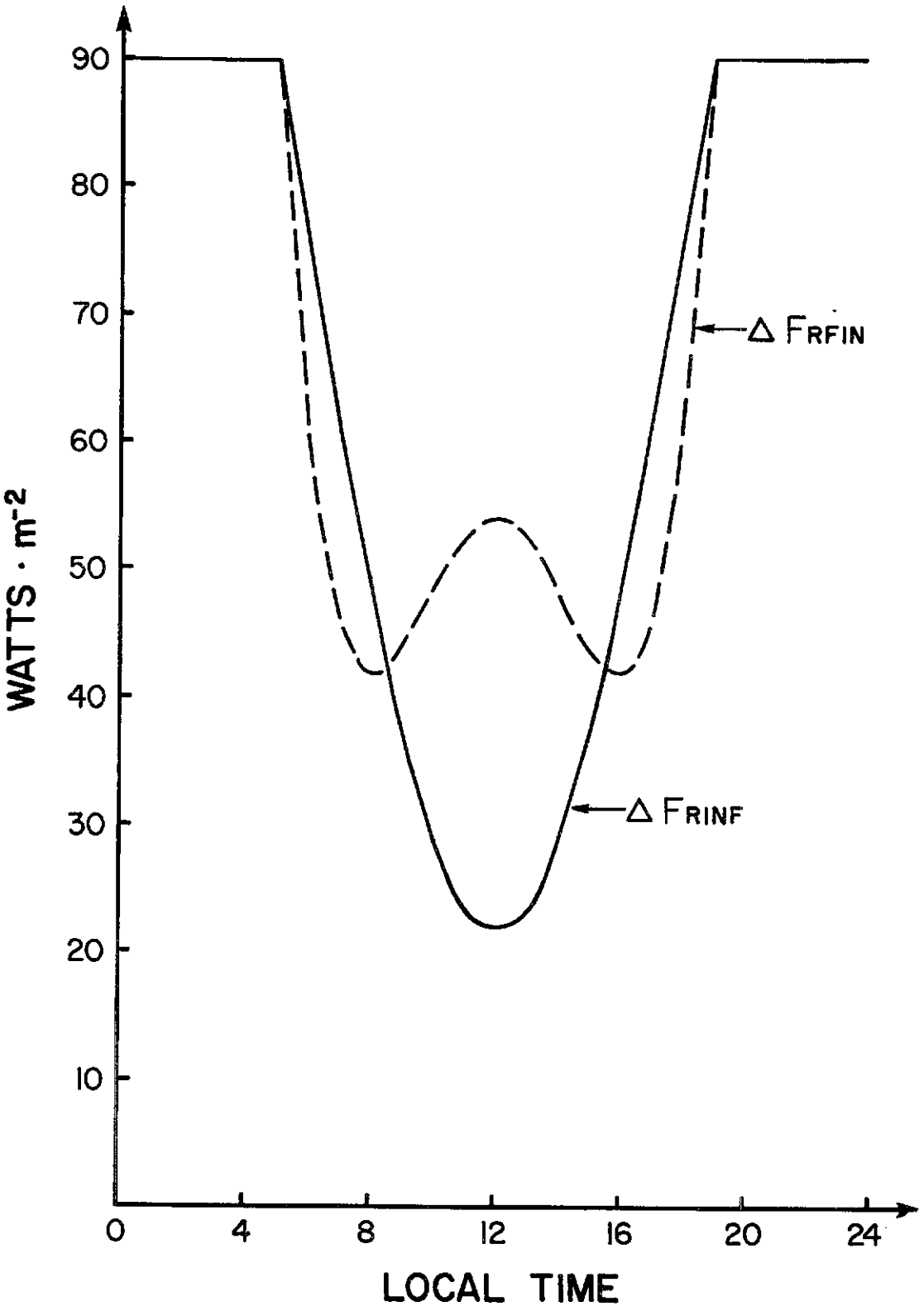

Figure 22. Net radiative fluxes for a stratocumulus cloud model if the cloud is considered horizontally homogeneous (solid) and if finite absorption characteristics are used (dashed).

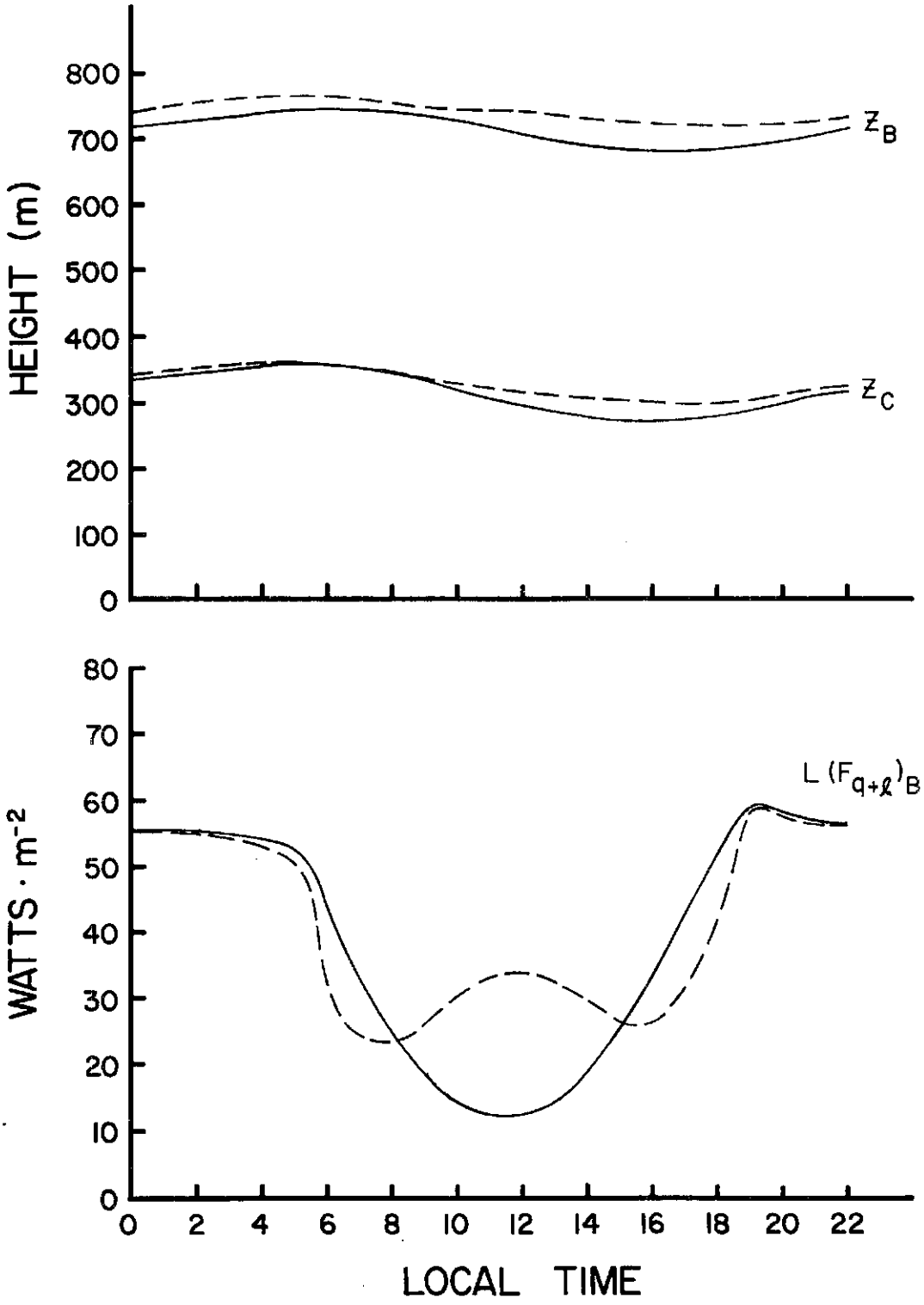

Figure 23. Diurnal variation of cloud thickness ($z_B - z_C$), top, and energy transport by total water L $(F_{q+\ell})_B$, (bottom), for infinite (solid) and finite (dashed) cloud absorption characteristics.

8.4 Effect of finite cloud characteristics on the daily shortwave radiative budget.

It has been shown that the effects of the finite cloud geometry on estimated directional reflectance values and surface solar irradiance values are zenith angle dependent, (see Sections 8.1 and 8.2). Consequently, the impact of the finite cloud characteristics on the daily shortwave radiative budget of a particular area must be evaluated by examining the time averaged role of the finite cloud geometry. In this section the time averaged disposition of incoming solar radiation is calculated for a hypothetical cloud field using both finite and infinite cloud properties and a comparison of the results is then made.

As a starting point the disposition of solar radiation for the finite, infinite and cloud free cases is presented in Table 15. The following assumptions have been made. The values of incident, reflected, absorbed and transmitted radiant power pertain to the column containing the parallel rays striking the finite and infinite cloud volumes. Thus, the horizontal cross-sectional area of the finite cloud's column is larger by the factor $(1 + \tan \theta)$, where θ is the solar zenith angle. The solar constant is assumed to be 1368 watts$\cdot$m^{-2}. Reflected radiation is calculated utilizing values of directional reflectance obtained from McKee and Cox (1974), combined with those of the present research. Rayleigh scattering is assumed to contribute 8% of the incident irradiance to the reflected component. The radiant power attributed to Rayleigh scattering is included in the amounts of reflected radiation. Absorption values refer to the radiant power absorbed above, in or below the cloud layer in the respective columns. Absorption is assumed

Cloud Thickness (m)	Solar Zenith Angle	Disposition of Solar Radiation	Power per unit area (watts·m^{-2})		
			Infinite	Finite	Clear
210	0°	Incident	1368.0	1368.0	1368.0
		Reflected	410.8	331.8	109.4
		Absorbed	351.8	361.1	325.8
		Transmitted	605.4	675.1	932.8
210	30°	Incident	1184.7	1184.7	1184.7
		Reflected	388.6	255.3	94.8
		Absorbed	310.5	313.6	289.2
		Transmitted	485.5	616.8	800.7
210	60°	Incident	684.0	684.0	684.0
		Reflected	288.5	169.8	54.7
		Absorbed	186.6	193.0	186.0
		Transmitted	208.9	321.2	443.2
630	0°	Incident	1368.0	1368.0	1368.0
		Reflected	671.2	532.2	109.4
		Absorbed	379.1	375.0	325.8
		Transmitted	317.7	460.7	932.8
630	30°	Incident	1184.7	1184.7	1184.7
		Reflected	605.0	395.9	94.8
		Absorbed	329.6	324.4	289.2
		Transmitted	250.1	464.3	800.7
630	60°	Incident	684.0	684.0	684.0
		Reflected	382.6	237.1	54.7
		Absorbed	193.7	196.0	186.0
		Transmitted	107.8	250.9	443.2

Table 15. Disposition of solar radiation for the 210 m (τ = 7.15) and 630 m thick (τ = 21.45) finite and infinite clouds and for the cloud free case, for solar zenith angles of 0°, 30° and 60°.

to be negligible at wavelengths less than 0.7 μm. The results are summarized for the 210 m and 630 m thick, finite and infinite clouds and also for the cloud free case for zenith angles of 0°, 30° and 60°.

Data from Table 15 are used in conjunction with the amount of fractional cloud cover to obtain values of fractional reflection, absorption and transmission for the region according to the following formulas,

$$\bar{x}_{inf} = x_{inf} \cdot f + x_{clr} \cdot (1-f), \text{ and}$$

$$\bar{x}_{fin} = x_{fin} \cdot f \cdot (1 + \tan \theta) + x_{clr} \cdot [1 - f (1 + \tan \theta)].$$

In the above formulas $\bar{x}_{inf}$ and $\bar{x}_{fin}$ represent the area averaged values of a parameter calculated using values of the parameter characteristic of infinite clouds, x_{inf}, or finite clouds x_{fin}. Also, f is the fractional cloud cover and θ is the solar zenith angle.

Table 16 shows values of fractional reflection, absorption and transmission for a cloud field over a totally absorbing surface, calculated using infinite cloud characteristics for a fractional cloud cover of 0.2. The 630 m thick (τ = 21.45) cloud characteristics are used.

Solar Zenith Angle	Fractional Reflection	Fractional Absorption	Fractional Transmission
0°	.16	.25	.59
30°	.17	.25	.58
60°	.18	.27	.55

Table 16. Values of fractional reflection, absorption and transmission using infinite cloud characteristics for a fractional cloud cover of 0.2 and zenith angles of 0°, 30° and 60°.

If finite cloud characteristics are used the results of Table 17 are obtained.

Solar Zenith Angle	Fractional Reflection	Fractional Absorption	Fractional Transmission
0°	.14	.25	.61
30°	.16	.25	.59
60°	.23	.28	.49

Table 17. Values of fractional reflection, absorption and transmission using finite cloud characteristics for a fractional cloud cover of 0.2 and zenith angles of 0°, 30° and 60°.

In order to obtain an average of the effects over an extended time period the values in Tables 16 and 17 are fitted as a function of zenith angle in terms of a parabolic equation. The equation is integrated over hour angle for a significant portion of the daylight period and an

average value obtained. Tables 18 to 20 show the time averaged values of radiant power per unit area reflected, absorbed and transmitted by an atmosphere populated by 20% sky cover of broken clouds calculated with the infinite and finite cloud results. The values are presented as a function of latitude for days corresponding to the equinox as well as the summer and winter solstices. Although the parabolic fit was determined for zenith angles less than 60°, some integrations at high latitudes include larger zenith angles and thus are extrapolations even though the hour angles were constrained to local times from 0800 to 1200.

The results indicate that in most cases the reflected component is greater when finite cloud results are used than when infinite cloud results are employed. This indicates that the solar zenith angle is at large enough values throughout a long enough segment of the averaging period so that the increased receipt of solar radiation by the finite cloud more than compensates for its lower value of directional reflectance. Only for 5° on the equinox and for 15°, 25° and 35° on the summer solstice is this not true. The values for time averaged atmospheric absorption are nearly equal with the finite cloud treatment absorbing a slightly greater amount in all cases. In contrast to the reflected component, the transmitted component is greater in the infinite treatment in almost all cases. This results from the increased shadow effect of the finite clouds at the large zenith angles which predominate in the averaging process. The results are presented in a slightly different form in Figures 24 to 26 as time averaged reflectivity, absorptivity and transmissivity values. The plots show the fraction of the average incoming solar radiation which is reflected, absorbed and transmitted. The most prominent feature of the graphs is

Latitude	Reflected Component (Infinite) in watts·m^{-2}	Reflected Component (Finite) in watts·m^{-2}	Abosrbed Component (Infinite) in watts·m^{-2}	Absorbed Component (Finite) in watts·m^{-2}	Transmitted Component (Infinite) in watts·m^{-2}	Transmitted Component (Finite) in watts·m^{-2}
5°	188.8	185.6	286.1	288.2	652.1	653.1
15°	184.1	184.9	278.6	281.2	630.1	626.6
25°	174.6	182.7	263.6	267.2	587.1	575.4
35°	160.4	177.6	241.2	245.9	525.2	503.2
45°	141.3	167.7	211.6	217.4	447.0	414.9
55°	117.6	150.5	175.1	181.5	356.2	316.9
65°	89.2	123.6	132.0	138.2	256.9	216.3
75°	56.5	84.7	83.0	87.9	153.3	120.2
85°	19.7	32.0	28.8	30.8	50.1	35.8

Table 18. Time averaged disposition of solar radiation for a 20% cloud covered totally absorbing surface using finite and infinite cloud characteristics for northern or southern hemisphere latitudes on the equinox.

Latitude	Reflected Component (Infinite) in watts·m^{-2}	Reflected Component (Finite) in watts·m^{-2}	Absorbed Component (Infinite) in watts·m^{-2}	Absorbed Component (Finite) in watts·m^{-2}	Transmitted Component (Infinite) in watts·m^{-2}	Transmitted Component (Finite) in watts·m^{-2}
5°	182.6	185.0	276.1	279.0	622.5	617.1
15°	191.3	187.0	289.9	291.9	662.1	664.4
25°	195.2	187.9	296.0	297.9	679.6	685.1
35°	194.2	188.4	294.4	296.3	674.1	678.0
45°	188.3	188.1	285.0	287.6	646.0	643.5
55°	177.6	186.2	267.9	271.7	596.4	584.1
65°	161.8	180.7	243.2	248.2	527.8	503.9
75°	141.1	169.6	211.1	217.2	443.2	408.6
85°	115.5	150.2	171.8	178.4	346.5	305.2

Table 19. Time averaged disposition of solar radiation for a 20% cloud covered totally absorbing surface using finite and infinite cloud characteristics for the summer solstice of the northern and southern hemispheres.

Latitude	Reflected Component (Infinite) in watts·m^{-2}	Reflected Component (Finite) in watts·m^{-2}	Absorbed Component (Infinite) in watts·m^{-2}	Absorbed Component (Finite) in watts·m^{-2}	Transmitted Component (Infinite) in watts·m^{-2}	Transmitted Component (Finite) in watts·m^{-2}
5°	168.9	180.6	254.6	258.6	562.5	546.7
15°	150.4	171.9	225.7	230.9	484.9	458.2
25°	127.0	156.4	189.6	195.6	393.2	357.7
35°	98.8	131.7	146.6	152.7	291.6	252.5
45°	66.0	95.2	97.3	102.5	184.6	150.2

Table 20. Time averaged disposition of solar radiation for a 20% cloud covered totally absorbing surface using finite and infinite cloud characteristics for the winter solstice of the northern and southern hemispheres.

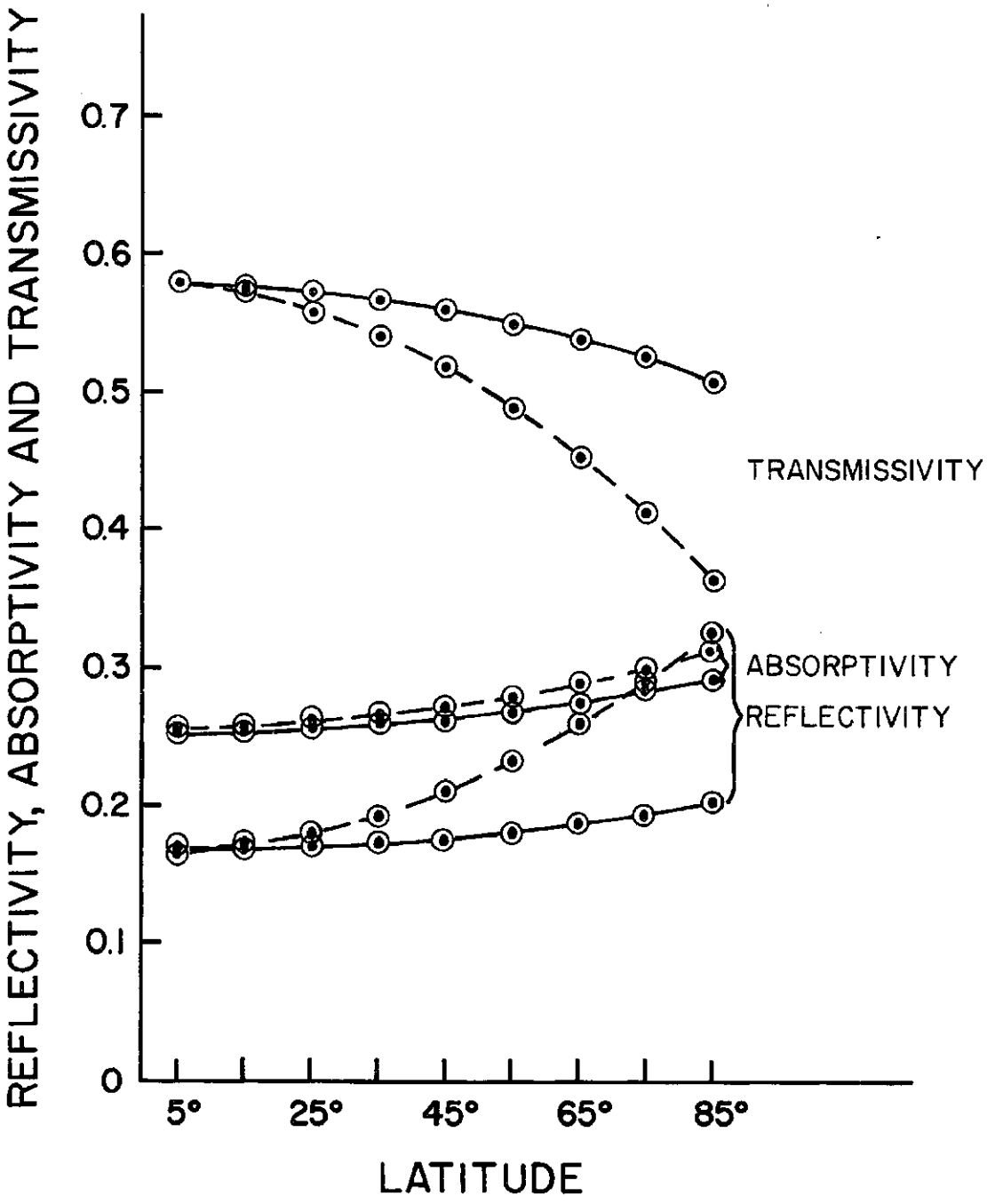

Figure 24. Average reflectivity, absorptivity and transmissivity for a totally absorbing surface with 20% cloud cover calculated with infinite (solid) and finite (dashed) cloud characteristics for northern and southern latitudes on an equinox.

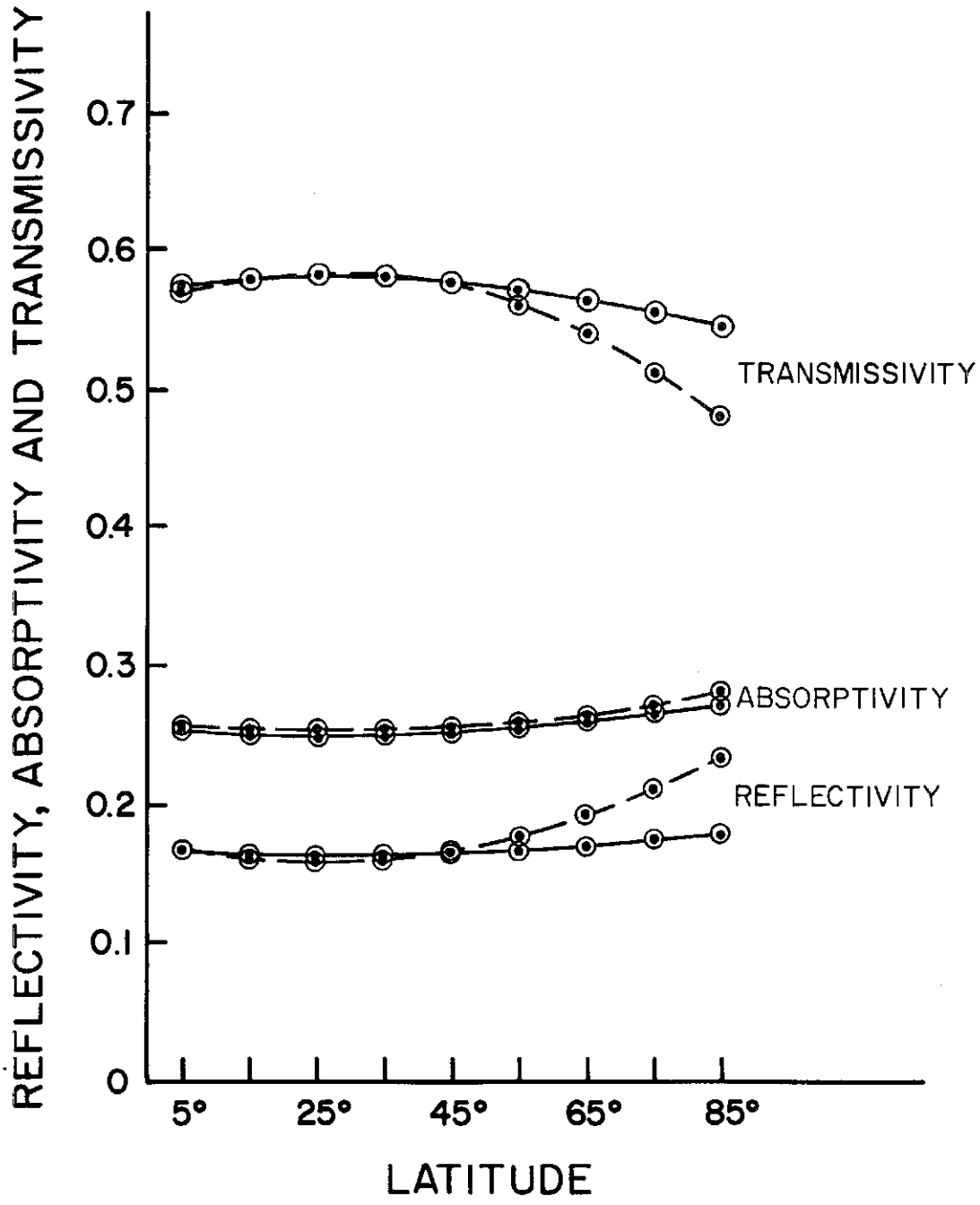

Figure 25. Average reflectivity, absorptivity and transmissivity for a totally absorbing surface with 20% cloud cover calculated with infinite (solid) and finite (dashed) cloud characteristics for the summer solstice.

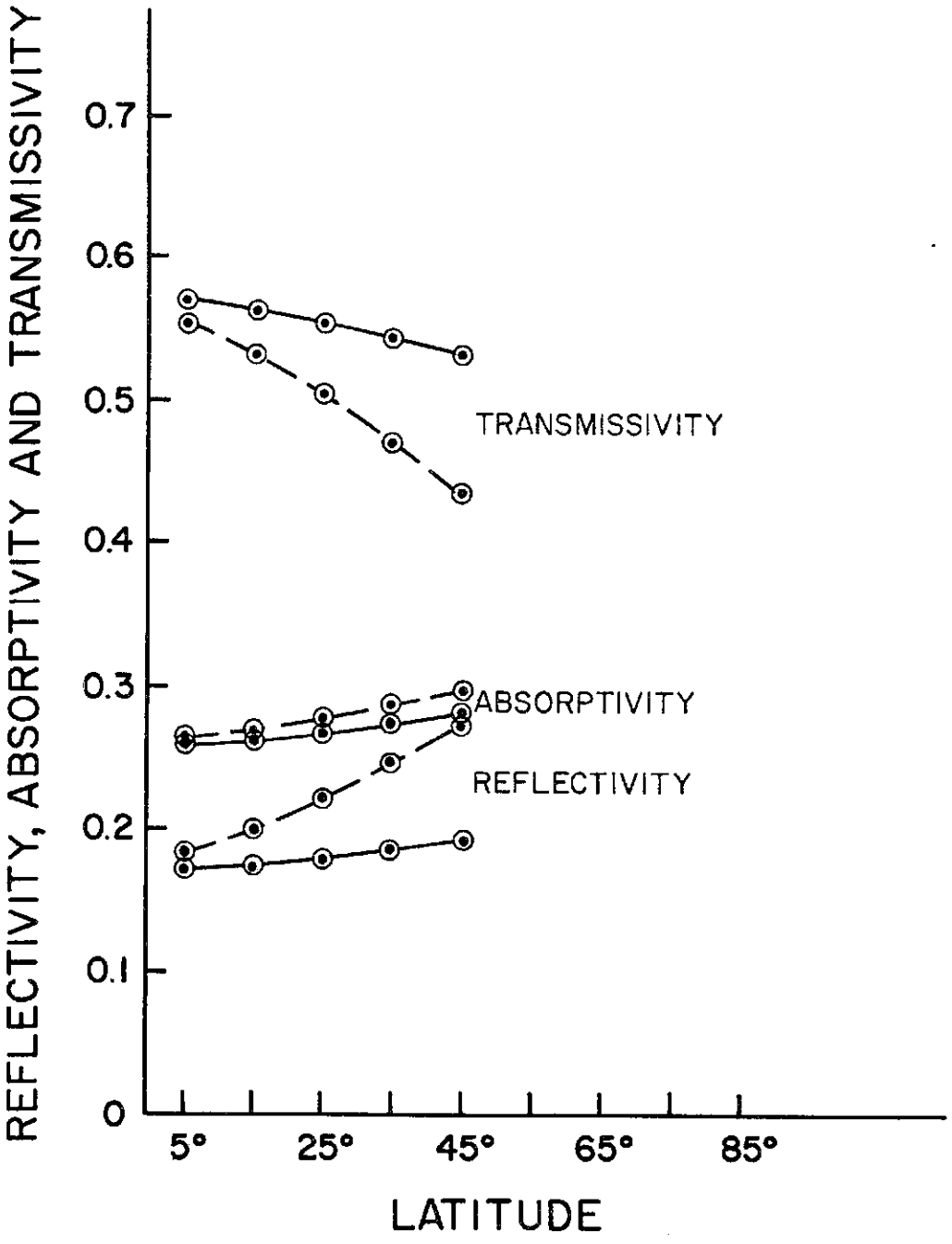

Figure 26. Average reflectivity, absorptivity and transmissivity for a totally absorbing surface with 20% cloud cover calculated with infinite (solid) and finite (dashed) cloud characteristics for the winter solstice.

the increased reflectivity and decreased transmissivity of the cloud field when treated with finite cloud results.

It is noted that a more detailed calculation may alter the above results. Inclusion of a non-zero surface albedo would have the effect of decreasing the relatively higher reflected component of the finite cloud field calculation. In fact, for large surface albedo, the finite cloud calculation may result in less reflected energy than for the infinite treatment, (see Section 8.1). Extension of the averaging period may act in the opposite sense since larger zenith angle behavior would then be included.

8.5 The importance of vertical and horizontal cloud dimensions for finite cloud radiative transfer calculations.

Several of the preceding sections have indicated that calculated values of reflectivity, absorptivity and transmissivity, using the finite cloud model, are dependent on the vertical extent of the cloud as well as the horizontal areal cover. The calculations in this research have all assumed a definite finite cloud geometry and have assumed that the horizontal cross-sectional area of the cloud was known. In this manner it was possible to formulate what has been termed "the adjusted fractional cloud cover" by multiplying the sky cover represented by the horizontal cross-sectional area of cloud cover by the factor $(1 + \tan \theta)$, where θ is the solar zenith angle. Obviously, it is not always possible to obtain an accurate estimate of the true horizontal cross-sectional area of cloud cover nor the vertical extent of cloud development. Ground observations indicate an amount of cloud cover which is derived from the magnitude of the horizontal cloud dimensions which must be differentiated from vertical cloud development

subject to the complication that almost all clouds are viewed at an angle. Even cloud cover estimates of finite clouds which are obtained from satellite observations do not give the correct horizontal cross-sectional cloud cover area. This can be seen in Figure 27 which depicts a geosynchronous satellite in relation to a single finite cubic cloud at latitude ϕ. If the cloud has sides of length ℓ, the satellite image appears to have an area given by

$$\text{Area} = \ell^2(\sin\phi + \cos\phi),$$

assuming that it is not possible to differentiate the vertical extent of the cloud from the horizontal dimension. In the same manner if a satellite views a field of such clouds whose true horizontal cross-sectional area comprises a fraction f of the total sky cover, then the satellite image will indicate a fraction f', where

$$f' = f\,(\sin\phi + \cos\phi).$$

Apparently then there are two geometrical factors which influence parameters calculated from finite cloud models. In the case of the cubic cloud these factors are functions of solar zenith angle and latitude. For clouds whose vertical and horizontal dimensions are not of equal magnitude, the ratio of horizontal dimension to vertical dimension is also important.

These two corrections can lead to a variety of different effects depending on cloud-sun geometry and cloud satellite geometry. While it is not the purpose here to explore these effects in detail, a computation

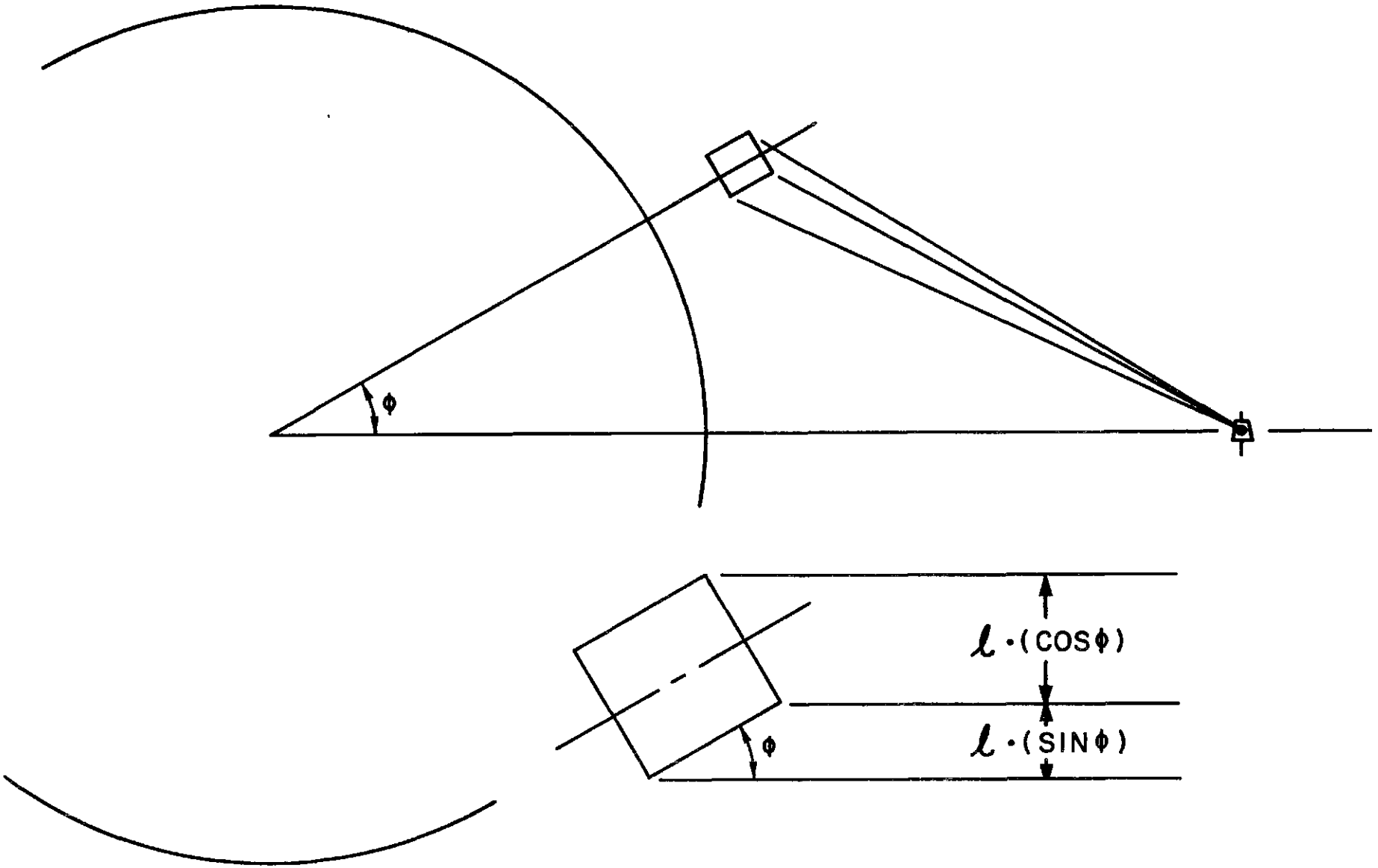

Figure 27. Depiction of geosynchronous satellite in relation to a single finite cloud at latitude ϕ and the amount of cloud cover which would be estimated from a satellite image.

is made which includes both correction factors. In order to facilitate comparison with the results of Section 8.4, it will be assumed that it is desired to calculate the reflected, absorbed and transmitted components of an area characterized by a totally absorbing surface underlying a cloud field whose true horizontal cross-sectional area constitutes 20% of the total sky area. Further, it is assumed that the apparent amount of cloud cover is estimated from information gathered by a geosynchronous satellite.

If such is the case the parameter $\bar{x}_{fin}$ which would actually be calculated using the estimate cloud cover is given by,

$$\bar{x}_{fin} = x_{fin} \cdot f \cdot (1 + \tan \theta)\ (\sin \phi + \cos \phi)$$

$$+ \ x_{clr} \cdot [1 - f\ (1 + \tan \theta)\ (\sin \phi + \cos \phi)],$$

where x_{fin} is the value of the parameter for an individual finite cloud, x_{clr} the value for the cloudless atmosphere, f the true cloud cover, θ the solar zenith angle and ϕ the latitude. Assuming that the indicated amount of cloud cover persists for a reasonable period of the day, we may, in an analogous fashion to section 8.4, obtain an average transmissivity, absorptivity and reflectivity by averaging over a considerable portion of the daylight hours. Figure 28 presents the results of such a computation as well as the results of the analogous case of Section 8.4. Again the 630 m thick (τ = 21.45) cloud results have been used. The calculations were made according to the solar geometry on the equinox. Although absorptivity values have not been greatly affected, reflectivity is especially enhanced in middle latitudes, while

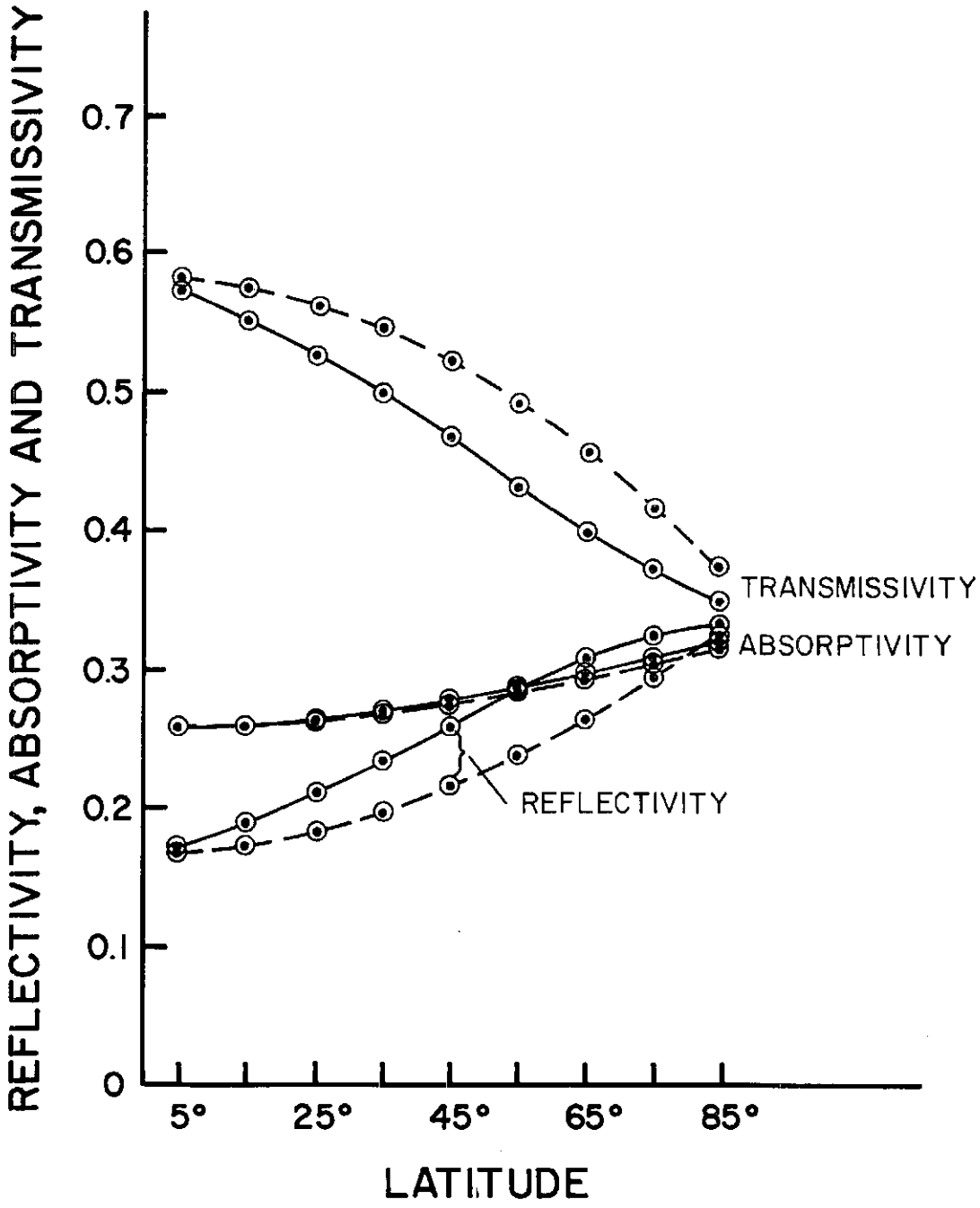

Figure 28. Time averaged reflectivity, absorptivity and transmissivity for a 20% cloud covered totally absorbing surface on the equinox calculated by the finite cloud model for true cloud cover (dashed) and cloud cover which would be derived from geosynchronous satellite imagery (solid).

transmissivity is diminished in a consistent manner.

The above results as well as those of section 8.4 point out the importance of considering vertical as well as horizontal cloud dimensions in calculations of the shortwave radiation budget in regions populated by fields of clouds whose horizontal and vertical dimensions are of similar magnitude.

8.6 Other areas of application

The previous sections have demonstrated the effects of finite cloud geometry on calculated values of directional reflectance, surface irradiance and absorption. These findings suggest that closer attention should be given to other topics upon which the finite cloud structure may have an important impact. For example, the finite cloud effects may play a significant role in the dispersal of ground fogs, which are usually treated as being horizontally homogeneous, but are often observed to be patchy in nature. Such effects may manifest themselves in two ways. First, the large zenith angles of the morning sun would indicate greater absorption by fog droplets in patchy fog than in a horizontally homogeneous medium. At small zeniths, the increased downward scattering by the finite cloud structures may create a greater amount of surface heating which would evaporate the fog from below. On a global scale, detailed investigation could include cloud interactions with other clouds and cloud interactions with the surface, especially in estimating the receipt of solar energy by the earth-atmosphere system in the tropics and subtropics. Parameters which may be affected are evaporation rates and heat storage in the oceans of this region of the globe. On a much smaller scale, the distribution of solar heating

in clouds for large zenith angles may be important in the initial stages of cloud growth. For larger clouds, the solar heating near the walls of the cloud may effect the properties of the air entrained into the cloud during the more rapid stages of growth. From a purely radiative point of view, properties of a growing cloud may prove interesting. Such a study could include variations of scattering and absorption properties in the vertical and horizontal for several stages of cloud growth. The list is certainly not exhaustive. Other areas of application will come to mind depending on the background of the reader.

9.0 CONCLUSIONS

A model for including the effects of water vapor and droplet absorption in finite cloud radiative transfer calculations has been described. The model has been utilized to examine the properties of reflected, absorbed and transmitted solar radiation, in the 0.7 μm to 8.0 μm region. The model has been applied to cubic, finite clouds, 210 m (τ = 7.15) and 630 m (τ = 21.45) on a side, and to volume elements of infinite clouds with identical dimensions for solar zenith angles of 0°, 30° and 60°. Comparison of the results leads to the following conclusions.

1. Ratios of directional reflectance, finite to infinite, in the conservative case decrease with increasing zenith angle from .77 at 0° to .51 at 60° for 210 m (τ = 7.15) thick cloud elements, and from .77 to .58 for 630 m (τ = 21.45) thick cloud elements, (see Table 4). The effect of water vapor and droplet absorptions within the cloud elements is to increase these ratios somewhat. As the zenith angle increases from 0° to 60°, the ratios decrease from .85 to .56 for the 210 m (τ = 7.15) thick clouds and from .87 to .62 for the 630 m (τ = 21.45) thick elements, (see Table 5). If water vapor absorption is included in the atmosphere above the cloud elements and also in the region surrounding the finite cloud, the ratios of directional reflectance decrease with increasing zenith angle from .74 at 0° to .48 at 60° for the 210 m (τ = 7.15) thick clouds, and from .78 at 0° to .56 at 60° for the 630 m (τ = 21.45) thick elements (see Table 6). Although the ratios of directional reflectance do not change greatly when absorption is included in the calculation, the individual values of directional

reflectance are reduced to approximately half of their conservative case values, (see Table 7).

2. Absorption of solar radiation within the 210 m (τ = 7.15) thick finite cloud ranges from 61% to 104% of the corresponding values in the infinite cloud element as the zenith angle increases from 0° to 60°. Absorption of solar radiation in the thicker 630 m (τ = 21.45) finite cloud is from 52% to 130% of the values calculated for the corresponding infinite volume element as the zenith angle increases from 0° to 60°, (see Table 9 and Figure 7).

3. The vertical and horizontal distribution of absorption in the two finite clouds has been examined for zenith angles of 0°, 30° and 60°. In the 0° zenith angle case, the maximum absorption in each of three layers of equal thickness is found in the center of the layers and the minimum near the corners. The average absorption in a given layer decreases from cloud top to cloud bottom. For the 30° and 60° zenith anlges the maximum absorption in each layer is near the middle of the row on the solar side and the minimum is near the corners on the anti-solar side, (see Figures 8 to 13).

4. Values of solar radiation absorbed by water vapor in the regions surrounding 210 m (τ = 7.15) and 630 m (τ = 21.45) thick finite clouds on the solar and anti-solar sides have been calculated. Results indicate that absorption of scattered photons is negligible in regions more than two cloud thicknesses away from the cloud, (see Figures 14 to 16).

5. Calculations of absorbed radiant power per unit area above the cloud volume elements show that the absorption above the 210 m (τ = 7.15) thick finite cloud ranges from 101% to 97% of the values above the

corresponding infinite cloud element as the zenith angle increases from 0° to 60°. In the 630 m (τ = 21.45) thick elements the values above the finite cloud range from 101% to 98% of the corresponding infinite cloud values for the same change in zenith angle, (see Table 10). The absorption values were normalized according to the horizontal cross-sectional area of the beam of parallel radiation incident on the two volume elements.

In terms of reflected radiant power absorbed above the cloud elements, values above the 210 m (τ = 7.15) thick finite cloud are from 100% to 250% of the values above the corresponding infinite cloud volume element as the zenith angle increases of 0° to 60°. For the 630 m (τ = 21.45) thick clouds the values in the finite case range from 111% to 194% of the corresponding infinite values for the same variation of zenith angle, (see Table 11).

6. When normalized according to the horizontal cross-sectional area of the cloud shadow, the radiant power per unit area absorbed below the 210 m (τ = 7.15) thick finite cloud is from 140% to 256% of the values for the 210 m thick infinite case as the zenith angle increases from 0° to 60°. For the thicker 630 m (τ = 21.45) clouds the values in the finite case are 272% to 509% of the values in the infinite case as the zenith angle increases from 0° to 60°, (see Table 12).

7. Calculated values of surface irradiance, for the 0.7 μm to 8.0 μm region, below the 210 m (τ = 7.15) thick finite cloud are from 111% to 164% of the values beneath the corresponding infinite clouds as the zenith angle is increased from 0° to 60°, when the values are normalized with respect to the horizontal areas of the respective cloud shadows. For the 630 m thick (τ = 21.45) cloud elements, surface

irradiance values beneath the finite cloud are 163% to 270% of the infinite cloud irradiance values, for the same variation of solar zenith angle. Including an approximation for the remainder of the shortwave spectrum does not significantly change these results, (see Tables 13 and 14).

8. The directional reflectance values have been used to calculate the directional reflectance values for a region characterized by a cloud field over a surface which contributes 5% to the directional reflectance in clear sky regions. Ratios of areal directional reflectances finite to infinite, range from .77 to 1.09 in the 210 m thick (τ = 7.15) case and from .75 to 1.30 in the 630 m (τ = 21.45) case, (see Figures 19 and 20).

9. Surface solar irradiance is estimated below a cloud field using finite and infinite cloud transmission properties. For a fractional cloud cover of less than 0.5, the finite and infinite calculations result in mean surface solar irradiance values which are within 5% of each other, for the 210 m (τ = 7.15), 0° zenith angle case as well as the 210 m (τ = 7.15) and 630 m (τ = 21.45) 30° zenith angle cases. For the same amount of cloud cover, the 630 m (τ = 21.45) 0° zenith angle values differ by more than 10%. At 0.3 sky cover differences of 10% and 20% are evident in values calculated for the 210 m (τ = 7.15) and 630 m (τ = 21.45) thick cases for a zenith angle of 60°, (see Figure 21).

10. Including finite cloud absorption effects in a cloud topped mixed layer model has been shown to have significant effects on the energy transport by total water predicted by such a model, (see Figure 23).

11. An accounting of the disposition of solar radiation in the atmospheric column which contains the cloud and its shadow as well as the parallel radiation striking the cloud shows the major role of the finite cloud is to reflect less and transmit more radiant power per unit area than the infinite cloud. Amounts of column absorption for the two cloud types are roughly equivalent, (see Table 15).

12. The time averaged disposition of solar radiation for a cloud field of 20% cloud cover over a totally absorbing surface indicates in general, that the reflected component is larger and the transmitted component smaller when finite cloud characteristics are used than when infinite cloud properties are used, with the absorbed component being nearly equal in both cases, (see Tables 18 to 20 and Figures 24 to 26).

13. The error in estimates of cloud cover obtained from geosynchronous satellite imagery is discussed pertaining to finite cloud radiative transfer calculations. The impact of such errors on time averaged values of reflectivity, absorptivity and transmissivity for a region with 20% finite cloud cover, overlying a totally absorbing surface, for the solar geometry of the equinox is calculated as a function of latitude. Reflectivity is overestimated and transmissivity underestimated, (especially in middle latitudes), while absorptivity is correctly given when such satellite imagery is utilized, (see Figures 27 and 28).

REFERENCES

Busygin, V.P., N.A. Yevstratov and Ye. M. Feygel'son, 1973. Optical properties of cumulus and radiant fluxes for cumulus cloud cover. Atmos. Oceanic Phys., 9, 1142-1151.

Howard, J.N., D.L. Burch, and D. Williams, 1956. Near-infrared transmission through synthetic atmospheres. J. Opt. Soc. Amer., 46, 186-190.

Liou, K.N., and T. Sasamori, 1975. On the transfer of solar radiation in aerosol atmospheres. J. Atmos. Sci., 32, 2166-2177.

McClatchey, R.A., R.W. Fenn, J.E.A. Selby, F.E. Volz, and J.S. Garing, 1971. Optical properties of the atmosphere. Environ. Res. Pap., No. 354, AFCRL.

McKee, T.B., and S.K. Cox, 1974. Scattering of visible radiation by finite clouds. J. Atmos. Sci., 31, 1885-1892.

_____, and S.K. Cox, 1976. Simulated radiance patterns for finite cubic clouds. J. Atmos. Sci., 33, 2014-2020.

Schubert, W.H., 1976. Experiments with Lilly's cloud-topped mixed layer model. J. Atmos. Sci., 33, 436-446.

Twomey, S., 1976. Computations of the absorption of solar radiation by clouds. J. Atmos. Sci., 33, 1087-1091.

Van Blerkom, D.J., 1971. Diffuse reflection from clouds with horizontal inhomogeneities. Astrophys. J., 166, 235-242.

Welch, R., J.F. Geleyn, W.G. Zdunkowski, and G. Korb, 1976. Radiative transfer of solar radiation in model clouds. Contributions to Atmos. Phys., 49, 128-146.

Wendling, P., 1977. Albedo and reflected radiance of horizontally inhomogeneous clouds. J. Atmos. Sci., 34, 642-650.

Zdunkowski, W.G., B.C. Nielsen, and G. Korb, 1967. Prediction and maintenance of radiation fog. Final Report, U. S. Army Electronics Command, Fort Monmouth, New Jersey, Contr. DAAB07-67-C-0049, 178 pp.

BIBLIOGRAPHIC DATA SHEET	1. Report No. CSU-ATSP-282	2.	3. Recipient's Accession No.
4. Title and Subtitle: Solar Absorption in Clouds of Finite Horizontal Extent			5. Report Date: January, 1978 6.
7. Author(s): John M. Davis, Stephen K. Cox and Thomas B. McKee			8. Performing Organization Rept. No. CSU-ATSP-282
9. Performing Organization Name and Address: Department of Atmospheric Science Colorado State University Fort Collins, Colorado 80523			10. Project/Task/Work Unit No. 11. Contract/Grant No. NSF & NOAA OCD -7421678 and ATM 77-15369
12. Sponsoring Organization Name and Address: Global Atmospheric Research Program National Science Foundation Washington, D.C. 20550			13. Type of Report & Period Covered: M.S. Thesis 14.

15. Supplementary Notes

16. Abstract: A model which includes the effects of water vapor and droplet absorption in finite cloud radiative transfer calculations is described. Total spectral (0.3 to 8.0 μm) values of directional reflectance of finite clouds are calculated and compared to values corresponding to horizontally infinite clouds of the same optical thickness. Absorption of solar radiation in finite clouds is compared to absorption in an equal volume element of horizontally infinite clouds. Absorptions above and below the geometrically different clouds are also compared as well as total spectral values of surface solar irradiance. Horizontally non-homogeneous values of absorption for the regions in and adjoining the finite cloud are presented. A total spectral, time and space averaged radiative budget is calculated for a totally absorbing surface partially covered by finite clouds. The results indicate that finite cloud effects have a significant impact on such calculations as a result of exposure of the vertical cloud wall to direct solar radiation. Additionally, it is shown that vertical development of finite clouds may have a significant impact on radiative budgets of regions partially covered by finite clouds, through enhancement of cloud cover estimates obtained from satellite imagery.

17. Key Words and Document Analysis. 17a. Descriptors

Finite cloud
Radiative transfer
Solar absorption
Directional reflectance
Cloud cover
Radiative budget

17b. Identifiers/Open-Ended Terms

17c. COSATI Field/Group

18. Availability Statement	19. Security Class (This Report) UNCLASSIFIED	21. No. of Pages 92
	20. Security Class (This Page) UNCLASSIFIED	22. Price

FORM NTIS-35 (10-70)